

TenCirChem: An Efficient Quantum Computational Chemistry Package for the NISQ Era

Weitang Li,^{*,†} Jonathan Allcock,[‡] Lixue Cheng,[†] Shi-Xin Zhang,[†] Yu-Qin Chen,[†]
Jonathan P. Mailoa,[†] Zhigang Shuai,^{¶,§} and Shengyu Zhang^{*,‡}

[†]*Tencent Quantum Lab, Shenzhen, 518057, China*

[‡]*Tencent Quantum Lab, Hongkong, 999077, China*

[¶]*Department of Chemistry, Tsinghua University, Beijing, 100084, China*

[§]*School of Science and Engineering, The Chinese University of Hong Kong, Shenzhen,
518172, China*

E-mail: liw31@gmail.com; shengyuzhang@tencent.com

Abstract

TENCIRCHEM is an open-source Python library for simulating variational quantum algorithms for quantum computational chemistry. TENCIRCHEM shows high-performance on the simulation of unitary coupled-cluster circuits, using compact representations of quantum states and excitation operators. Additionally, TENCIRCHEM supports noisy circuit simulation and provides algorithms for variational quantum dynamics. TENCIRCHEM’s capabilities are demonstrated through various examples, such as the calculation of the potential energy curve of H₂O with a 6-31G(d) basis set using a 34-qubit quantum circuit, the examination of the impact of quantum gate errors on the variational energy of the H₂ molecule, and the exploration of the Marcus inverted

region for charge transfer rate based on variational quantum dynamics. Furthermore, TENCIRCHEM is capable of running real quantum hardware experiments, making it a versatile tool for both simulation and experimentation in the field of quantum computational chemistry.

1 Introduction

Quantum computation leverages quantum effects to store and process data, which could lead to a revolution in computational chemistry.¹⁻⁵ With the advent of noisy intermediate scale quantum (NISQ) computing⁶, devices with tens of error-prone qubits are increasingly becoming available for use to researchers and the public.⁷⁻¹⁰ Since such devices are not capable of running large-depth structured quantum algorithms, the question of how to best utilize them to solve chemistry problems is of deep scientific and commercial significance. In recent years, following pioneering proposals such as the variational quantum eigensolver (VQE),¹¹ research has focused on variational algorithms based on parameterized quantum circuits (PQC).¹²⁻¹⁴ In the long term, the quantum phase estimation (QPE) algorithm offers a promising route to evaluating the energy of molecular systems, as it may potentially provide an exponential advantage over classical full configuration interaction (FCI) treatment.^{15,16} However, compared with VQE, the circuit depths required to run QPE are typically far too deep to run on near-term quantum devices, making VQE the approach of choice in the NISQ era.

VQE uses a parameterized quantum circuit to represent a system’s wavefunction and works by tuning the circuit parameters to minimize the energy variationally. In this setting, the quantum circuit plays the same role as the ansatz in classical quantum chemistry algorithms and, similarly, a variety of different ansätze have been proposed. The first such proposal was the disentangled unitary coupled cluster (UCC) ansatz,¹¹ which is a variant of the classical coupled cluster method. While disentangled UCC differs from the traditional UCC ansatz developed for classical computers,^{17,18} for brevity, in the following, we

will omit the word “disentangled”. UCC is known to be difficult to implement in classical computers, yet the ansatz can be transformed into a PQC straightforwardly¹⁹ and implemented on a quantum computer. While excitations are commonly restricted to single and double excitations – a case referred to as UCCSD – a number of other variants of UCC have also been proposed.^{20–22} Another popular family of ansätze is the hardware-efficient ansatz (HEA),²³ which is designed to be first and foremost easily implementable on a target quantum hardware platform, and includes fewer quantum chemistry heuristics compared to UCC. In addition to ground state properties, such as molecular energy, chemists are also interested in quantum dynamics.²⁴ Under the PQC framework, the time evolution of the circuit parameters can be determined using time-dependent variational principles.^{25,26}

While the quality and availability of quantum computing hardware continue to improve, the majority of real experiments are currently still constrained to small numbers of qubits and very shallow circuits.^{23,27–31} Furthermore, optimizing circuit parameters on real devices is challenging: gradient-based methods are inefficient, as they rely on computing finite differences or parameter-shifts,^{32,33} and both gradient and gradient-free methods are susceptible to noise. These factors mean that, for the foreseeable future, the classical simulation of variational quantum algorithms will play an important role in studying and analyzing their performance and viability. Although a variety of simulation software is currently available, there remain opportunities to significantly improve efficiency, functionality, and flexibility.

Here we introduce TENCIRCHEM, an efficient open-source Python library for simulating variational quantum chemistry algorithms, designed to be easy to use as a black box while allowing for a high degree of flexibility and customizability. TENCIRCHEM is powered by TENSORCIRCUIT,³⁴ a recently released quantum circuit simulation package featuring an advanced tensor network contraction simulation engine. A recently developed algorithm to efficiently simulate the UCC ansatz on classical computers^{35–37} is also implemented in TENCIRCHEM with notable performance optimizations. We demonstrate how to use TENCIRCHEM by providing concrete code snippets, as well as links to online tutorials for features,

such as efficient UCC calculation, noisy circuit simulation, and quantum dynamics simulation. In the examples, we include an accurate UCCSD potential energy curve of the water molecule corresponding to 34 qubits, the influence of quantum gate error rate and measurement shots on VQE energy, the spin relaxation dynamics of the spin-boson model, and much more.

The paper is structured as follows. In the rest of the section, we briefly review variational quantum algorithms for quantum chemistry and existing simulation packages. In Sec. 2, we present the overall architecture and workflow of TENCIRCHEM with an emphasis on related theoretical background. Secs. 3, 4, and 5 illustrate the features contained in the TENCIRCHEM modules through code snippets and detailed simulation examples.

1.1 Variational quantum algorithms for quantum chemistry

Variational quantum algorithms for quantum chemistry have been an active area of research since the original VQE proposal.¹¹ For both ground state properties and quantum dynamics, while details vary, proposed protocols typically adhere to the following workflow:

Input. The input to the problem is the system Hamiltonian in second-quantized form. For electronic structure problems, this can be expressed as

$$H = \sum_{pq} h_{pq} a_p^\dagger a_q + \frac{1}{2} \sum_{pqrs} h_{pqrs} a_p^\dagger a_q^\dagger a_r a_s + E_{\text{nuc}}, \quad (1)$$

where h_{pq} and $h_{pqrs} = [ps|qr]$ are one-electron and two-electron integrals, and a_p^\dagger, a_p are fermionic creation and annihilation operators, respectively, acting on the p -th spin-orbital. E_{nuc} is the nuclear repulsion energy. For quantum dynamics simulations, the Hamiltonian varies from system to system, and may contain only electronic terms^{38,39} or both electronic and vibrational terms.^{40,41} The latter is referred to as vibronic-coupling Hamiltonians.

Conversion to qubits. The Hamiltonian, either electronic or vibronic-coupling, is converted into an N -qubit Hamiltonian of the form

$$H = \sum_j^M \alpha_j P_j, \quad (2)$$

where the α_j are real coefficients, M is the total number of terms, and the P_j are Pauli strings of the form $P_j = \sigma_{i_1} \otimes \sigma_{i_2} \otimes \dots \sigma_{i_N}$ where the σ_{i_k} are single qubit Pauli operators or the identity. For electronic Hamiltonians, the Jordan-Wigner transformation,⁴² parity transformation^{43,44} and Bravyi-Kitaev transformation⁴⁴ are popular choices to perform this conversion. The Jordan-Wigner and Bravyi-Kitaev transformations require one qubit per spin-orbital, while the parity transformation is able to save 2 qubits, relative to these other methods, due to electron number conservation in each spin sector. For vibronic-coupling Hamiltonians, the nuclear states also need to be encoded into qubits via unary or binary encodings.⁴⁵

Choice of ansatz. A parameterized ansatz state $|\psi(\theta)\rangle = U(\theta) |\psi_0\rangle$ is selected, where $U(\theta)$ is the unitary corresponding to a quantum circuit characterized by a vector θ of tunable parameters, and $|\psi_0\rangle$ is a chosen reference state or initial state. The core role of quantum computers or quantum processing units (QPUs) in variational algorithms is to use quantum circuits to execute $U(\theta)$ and prepare $|\psi(\theta)\rangle$. Thus, the ability of the variational ansatz in expressing the system wavefunction is a key factor impacting the accuracy of variational quantum algorithms for quantum chemistry. For electronic Hamiltonians, the proposed ansätze generally fall into unitary coupled cluster (UCC) based approaches,^{11,21,46–48} and hardware-efficient ansätze.^{23,27–31} For quantum dynamics simulation, the appropriate family of ansatz varies from system to system. The variational Hamiltonian ansatz^{49,50} and adaptive ansatz⁵¹ automate the task of constructing problem-specific circuit ansätze.

Updating parameters. In the case of VQE, because the true ground state energy E_0 of the system gives a lower bound on the energy expectation value $\langle H \rangle_\theta := \langle \psi(\theta) | H | \psi(\theta) \rangle$, $\langle H \rangle_\theta$ is minimized with respect to the parameters θ , which in turn gives an upper bound on E_0 i.e.,

$$E_0 \leq \min_{\theta} \langle H \rangle_\theta.$$

The quality of this bound depends on the chosen ansatz. In general, the function is non-convex and one can only expect to find a local minimum, which depends on the parameter initializations and the optimization protocol used. For dynamics problems, the parameters are propagated according to time-dependent variational principles, of which McLachlan's variational principle is among the most popular choices for quantum computing.^{26,52} McLachlan's variational principle minimizes the distance between the ideal time derivative $-iH |\psi(\theta)\rangle$, i.e. and actual time derivative $\frac{\partial}{\partial t} |\psi(\theta)\rangle$

$$\min_{\dot{\theta}} \left\| \left(\frac{\partial}{\partial t} + iH \right) |\psi(\theta)\rangle \right\|. \quad (3)$$

At each time step, $\dot{\theta} = \frac{\partial \theta}{\partial t}$ is solved and then θ is evolved numerically according to $\dot{\theta}$. The equation of motion for θ_k , the k th element in vector θ , is

$$\sum_k M_{jk} \dot{\theta}_k = V_j, \quad (4)$$

where

$$M_{jk} = \text{Re} \left\{ \frac{\partial \langle \psi |}{\partial \theta_j} \frac{\partial | \psi \rangle}{\partial \theta_k} \right\}, \quad V_j = \text{Im} \left\{ \frac{\partial \langle \psi |}{\partial \theta_j} H | \psi \rangle \right\} \quad (5)$$

Both M_{jk} and V_j can be evaluated on a quantum computer with one additional ancilla qubit via the Hadamard test.²⁵ $\dot{\theta}_k$ can then be deduced using a standard linear equation solver on a classical computer. After that, θ_k is propagated in time with time step τ either by the simple forward Euler method $\theta_k(t + \tau) = \theta_k(t) + \tau \dot{\theta}_k(t)$ or more sophisticated initial value

problem solvers, such as Runge-Kutta solvers.

1.2 Existing packages: Challenges and opportunities

A number of useful software packages are currently available, which facilitate the research, design, and validation of quantum computational chemistry algorithms. A variety of general quantum computing packages, such as QISKIT,⁵³ PENNYLANE,⁵⁴ and MINDQUANTUM,⁵⁵ have modules or sub-packages dedicated to chemistry applications, and there are also standalone quantum simulation packages that are mostly or completely designed for quantum computational chemistry, such as TEQUILLA,⁵⁶ Q² CHEMISTRY,⁵⁷ and QFORTE.⁵⁸

The efficiency and scalability of the packages depend crucially on the underlying circuit simulation algorithm. The most commonly encountered quantum circuit simulator is statevector simulator, which is implemented in all simulation packages mentioned above. By using statevector simulator, all (exponentially many with respect to the number of qubits) amplitudes of the wavefunction are computed and stored. For such simulators, the largest simulated UCC circuit to date contains fewer than 30 qubits.⁵⁹ In contrast, matrix product state (MPS) simulators are able to tackle larger circuits, with around 100 qubits^{60,61} possible. Among the packages mentioned above, QISKIT, PENNYLANE, and Q² CHEMISTRY have implemented the MPS simulator. However, MPS simulation involves approximations which could be problematic for the validation of quantum algorithms. Another challenge for software development is noisy circuit simulation and interfacing with hardware. These features can help researchers better understand the behavior of quantum algorithms in real-world conditions, facilitating the development of noise-resilient quantum algorithms and better error mitigation techniques,^{47,50,62} which are essential for building practical quantum computers. QISKIT is currently the only package capable of noisy circuit simulation and interfacing with quantum hardware. Furthermore, to the best of the authors' knowledge, quantum dynamics algorithms of molecular systems are not implemented in any packages currently available.

TENSORCIRCUIT is a recent open-source quantum circuit simulator based on tensor network contraction which – in certain cases – enables the simulation of up to 600 qubits without any approximation.³⁴ Differences between tensor network contraction simulators and MPS simulators are described in Sec. 2.4. TENSORCIRCUIT is built upon industry-leading machine learning frameworks, such as JAX⁶³ and employs automatic differentiation (AD), just-in-time (JIT) compilation, and vectorized parallelism to accelerate simulation. TENSORCIRCUIT also possesses a fully-fledged noise model which enables efficient noisy circuit simulation. With its TENSORCIRCUIT backend, TENCIRCHEM provides a competitive option for developing and analyzing quantum computational chemistry algorithms. The role of TENSORCIRCUIT in TENCIRCHEM is described in more detail in Sec. 2.1.

2 TenCirChem Overview and Theoretical Backgrounds

In this section, we provide a high-level picture of TENCIRCHEM by introducing its architecture and typical workflow. In addition, we present the theoretical background relevant to the code examples found in Secs. 3, 4 and 5.

2.1 Architecture and workflow

Architecture. TENCIRCHEM consists of two primary modules (Fig. 1), corresponding to (i) electronic structure and (ii) quantum dynamics. Both modules contain a set of pre-built ansätze, and user-specified custom ansätze are also supported. Due to the popularity and unique mathematical structure of the UCC ansatz, an efficient simulation engine "civector" is implemented specifically for its efficient simulation. The details of the engine are included in the Supporting Information. In short, the engine exploits particle number conservation to store the system wavefunction in *configuration interaction vector* ("civector") form and uses *UCC factor expansion* to accelerate simulation. This engine relies heavily

on the FCI module of PySCF⁶⁴ for the construction and manipulation of the configuration interaction vector. In addition, the gradient is evaluated by auto-differentiation with reversible computing, which is more memory-efficient than the traditional reverse-mode auto-differentiation implemented in standard machine-learning packages.⁶⁵ The "tensornetwork" engine uses the TENSORCIRCUIT tensor network contraction kernels to perform circuit simulation. A variant of the "tensornetwork" engine is the "tensornetwork-noise" engine, which further includes circuit gate noise and measurement uncertainty in the simulation using the relevant utilities implemented in TENSORCIRCUIT. The "qpu" engine delegates circuit execution to real QPUs through TENSORCIRCUIT.

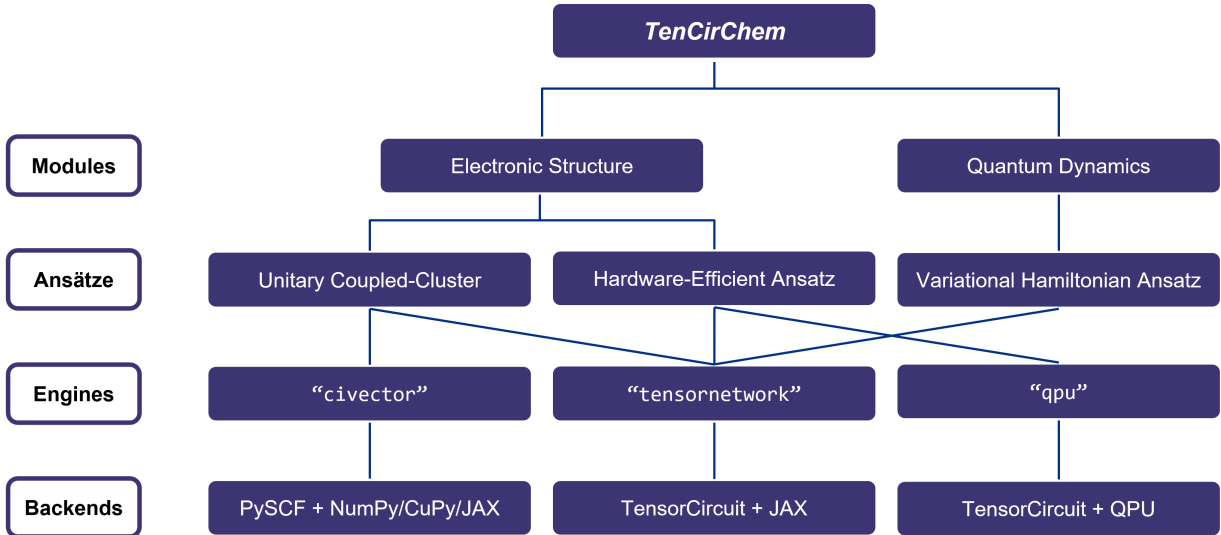


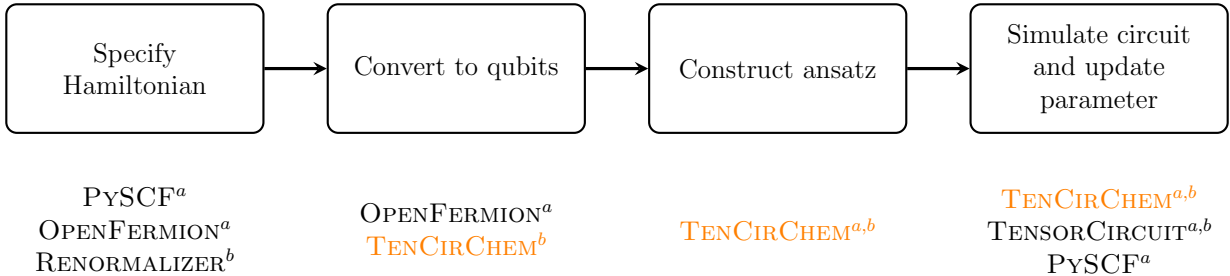
Figure 1: The architecture of TENCIRCHEM. The electronic structure and quantum dynamics modules are described in depth in Secs. 3, 4 and 5. See Sec. 2.3 for more information on the supported ansätze. For more details on engines and backends see Sec. 2.4.

Workflow. As mentioned in the introduction, the starting point for variational quantum chemistry algorithms is normally taken to be the Hamiltonian in the second-quantized form. For electronic structure problems, this means specifying the one- and two-electron integrals h_{pq} and h_{pqrs} in Eq. 1. In TENCIRCHEM this can be done either directly, by inputting these numbers explicitly, or indirectly, by specifying the 3D coordinates, atom types, and basis sets

of each of the atoms in a molecule and having PYSCF compute the integrals automatically. The Hamiltonian in quantum dynamics is defined using the RENORMALIZER⁶⁶ package by specifying each term in the Hamiltonian.

Next, the Jordan-Wigner, parity or Bravyi-Kitaev conversion from electronic Hamiltonian (Eq. 1) to qubit Hamiltonian (Eq. 2) is performed by OPENFERMION.⁶⁷ The encoding of nuclear states to qubits and the construction of the ansätze are performed within the TENCIRCHEM package. The workflow and the underlying packages are summarized in Fig. 2, in accordance with Sec. 1.1, and will be elaborated on in the following sections. Standard infrastructure packages, such as NUMPY and SCIPY, are omitted for brevity. The specific tasks of each underlying package are summarized below:

- PYSCF: specifying molecules; calculating integrals; configuration interaction vector construction and manipulation.
- OPENFERMION: specifying operators in fermion operator or qubit operator format; conversion from fermion operator to qubit operator.
- RENORMALIZER: specifying general quantum dynamics Hamiltonian; conversion from symbolic operators to numeric operators.
- TENSORCIRCUIT: constructing custom PQC as ansatz; quantum circuit simulation via tensor network contraction; interfacing with QPU.



^aFor electronic structure. ^bFor quantum dynamics.

Figure 2: Typical workflow of variational quantum algorithms and the underlying packages used for each task in TENCIRCHEM.

2.2 Conversion to qubits

Quantum simulation of physical systems requires converting fermions (for electronic structure calculations) and bosons (for encoding nuclear wavefunctions and quantum dynamics) to qubits.

2.2.1 Electronic Structure

Fermionic creation and annihilation operators obey the anticommutation properties

$$\begin{aligned}\{a_i, a_j^\dagger\} &= a_i a_j^\dagger + a_j^\dagger a_i = \delta_{ij} \\ \{a_i^\dagger, a_j^\dagger\} &= \{a_i, a_j\} = 0\end{aligned}\tag{6}$$

while the qubit creation operator $c^\dagger = \frac{1}{2}(X - iY)$ and annihilation operator $c = \frac{1}{2}(X + iY)$ obey the commutation properties

$$\{c_i, c_j^\dagger\} = \delta_{ij}, \quad [c_i^\dagger, c_j^\dagger] = [c_i, c_j] = 0.\tag{7}$$

To comply with the required fermionic anticommutation properties, the Jordan-Wigner transformation⁴² can be used to map fermionic ladder operators into products of Pauli Z and qubit ladder operators

$$a_j = \bigotimes_{l=0}^{j-1} Z_l \otimes c_j.\tag{8}$$

Alternatively, the parity transformation^{43,44} achieves the same goal by letting each qubit record the parity of all preceding orbitals and itself. The mapping is then

$$a_j = (c_j \otimes |0\rangle \langle 0|_{j-1} - c_j^\dagger \otimes |1\rangle \langle 1|_{j-1}) \otimes \bigotimes_{l=j+1}^{N-1} X_l\tag{9}$$

where N is the total number of qubits. If the ansatz conserves the total particle number, then the last qubit will not change during computation and can be removed without loss of

accuracy. If S_z is also conserved, another qubit can be saved. Thus, the parity transformation uses 2 fewer qubits than the Jordan-Wigner transformation. In `TENCIRCHEM`, both transformations are carried out by calling `OPENFERMION`.

2.2.2 Quantum Dynamics

One of the key differences between quantum dynamics simulation and electronic structure calculations is that quantum dynamics requires incorporating nuclear information in time evolution. Similar to the case of electrons, a proper basis set must first be chosen to represent the nuclear wavefunction and operators in second-quantized form.^{40,62,68} One popular choice is the harmonic eigenbasis, in which the nuclear position operator x and momentum operator p are expressed as

$$\begin{aligned} x &= \sqrt{\frac{1}{2m\omega}}(b^\dagger + b), \\ p &= i\sqrt{\frac{m\omega}{2}}(b^\dagger - b), \end{aligned} \tag{10}$$

where m is the oscillator mass, ω is the oscillator frequency and b^\dagger (b) are bosonic creation (annihilation) operators respectively. The infinite boson levels are then truncated to the lowest N levels for further encoding. Other choices for the nuclear basis set include the real-space grid basis and a variety of discrete value representations.⁶⁹ In any case, each nuclear degree of freedom is represented by a finite number of basis states $|\psi\rangle = \sum_i^N c_i |i\rangle$.

In quantum simulation, each bosonic basis vector $|i\rangle$ must be encoded into qubits, so that the system wavefunction can be described by a quantum circuit and operators can be represented by Pauli strings. The principle for the encoding is equivalent to that of encoding integers into bit strings, and there are two common encoding strategies – based on unary and binary encodings – requiring $\mathcal{O}(N)$ and $\mathcal{O}(\log N)$ qubits, respectively.⁴⁵ Binary encoding with Gray codes is a variant of the standard binary encoding that involves changing only one bit between consecutive integers, which can be used to facilitate the efficient encoding of operators b^\dagger and b . `TENCIRCHEM` supports all of the encoding schemes and by default

uses binary encoding with Gray codes because of its compact representation. We note that an efficient variational encoding scheme requiring only $\mathcal{O}(1)$ qubits was proposed recently.⁷⁰

2.3 Supported ansätze

TENCIRCHEM supports three classes of variational ansätze: (i) Unitary Coupled Cluster (UCC) – of which UCCSD, k -UpCCGSD, and paired UCCD (pUCCD) are variants –, (ii) Hardware-Efficient, and (iii) Variational Hamiltonian.

2.3.1 Unitary Coupled Cluster Ansatz

UCC ansätze have the form

$$e^{T(\theta)} |\phi\rangle \tag{11}$$

where

$$T(\theta) = \sum_{pq} \theta_{pq} (a_p^\dagger a_q - \text{h.c.}) + \sum_{pqrs} \theta_{pqrs} (a_p^\dagger a_q^\dagger a_r a_s - \text{h.c.}) \dots, \tag{12}$$

θ denotes the vector of tunable parameters $\theta_{pq}, \theta_{pqrs}, \dots$, and $|\phi\rangle = |\text{HF}\rangle$ is the Hartree–Fock state. In general, excitations of any order are permitted, although it is common to only consider single and double excitations, in which case the ansatz is referred to as UCCSD. The indices are usually confined to excitations from occupied orbitals to virtual (unoccupied) orbitals. “Generalized” excitations do not have to satisfy this requirement. The generalized counterpart of UCCSD is UCCGSD.²⁰

As the terms in Eq. 12 do not necessarily commute, the exact implementation of Eq. 11 on a gate model quantum computer is difficult. In fact, to the best of our knowledge the ansatz defined by Eq. 11 and Eq. 12 is never used in any practical VQE algorithm. Instead, one considers a Trotterized approximation of the ansatz, also referred to as disentangled UCC.⁷¹

Although disentangled UCC is traditionally viewed as an approximation to the original UCC, it can in fact exactly represent general fermionic states given appropriate operator ordering and should probably be considered as an alternative ansatz to the original UCC.⁷¹ In general, the disentangled UCC ansatz can be written as

$$|\Psi(\theta)\rangle_{\text{UCC}} := \prod_{k=N_{\text{ex}}}^1 e^{\theta_k G_k} |\phi\rangle, \quad (13)$$

where each G_k is the anti-Hermitian excitation operator for each term in Eq. 12, and N_{ex} is the total number of excitations. In the following, the terms $e^{\theta_k G_k}$ are referred to as UCC factors. The UCC ansätze implemented in TENCIRCHEM can all be viewed as special cases of Eq. 13. The specific formulation of UCCSD, k -UpCCGSD, and pUCCD are reviewed in the Supporting Information.

2.3.2 Hardware-Efficient Ansatz

Hardware-efficient ansätze are designed to be easily implementable on NISQ devices but do not necessarily preserve symmetries in molecular systems. Finding the global minimum for such circuits can be challenging due to the vanishing gradient phenomenon and the presence of local minima.^{72,73} However, because the required circuit depths can be much smaller than for UCC, hardware-efficient ansätze are widely used in quantum computational chemistry experiments performed on real quantum processors.^{23,27–31} TENCIRCHEM implements one of the most popular hardware-efficient ansätze, the R_y ansatz,^{30,73–75} whose circuit consists of interleaved layers of R_y and CNOT gates

$$|\Psi(\theta)\rangle_{R_y} := \prod_{l=k}^1 \left[L_{R_y}^{(l)}(\theta) L_{\text{CNOT}}^{(l)} \right] L_{R_y}^{(0)}(\theta) |\phi\rangle, \quad (14)$$

where k is the total number of layers, and the layers are defined as

$$\begin{aligned} L_{\text{CNOT}}^{(l)} &= \prod_{j=N-1}^1 \text{CNOT}_{j,j+1}, \\ L_{R_y}^{(l)}(\theta) &= \prod_{j=N}^1 \text{RY}_j(\theta_{lj}). \end{aligned} \tag{15}$$

The gate subscripts refer to the qubit index on which the gate acts and N is the total number of qubits. An example of the ansatz is depicted in Fig. 6. One reason for using the R_y gate is that it enforces the wavefunction coefficients to be real, which is a desired property for electronic structure problems.

As a huge number of possible hardware-efficient ansätze can be defined, instead of providing templates for all of them, TENCIRCHEM allows the hardware-efficient ansätze from the QISKIT library to be directly imported, and other customized ansätze can be defined by the user using TENSORCIRCUIT (see Sec. 4.1 for examples).

2.3.3 Variational Hamiltonian Ansatz

For quantum dynamics simulations, TENCIRCHEM provides utilities to construct the variational Hamiltonian ansatz^{49,50} based on user-specified Hamiltonians. This type of ansatz depends on the Pauli strings P_j contained in the Hamiltonian and thus encodes Hamiltonian information. Suppose the Hamiltonian is composed of M Pauli strings P_j , as defined in Eq. 2. The corresponding variational Hamiltonian ansatz has the form

$$|\Psi\rangle = \prod_l^k \prod_j^M e^{-i\theta_{lj}P_j} |\phi\rangle, \tag{16}$$

where $|\phi\rangle$ is the initial state of the system, θ_{kj} is the circuit parameter, and k is a parameter defining the number of layers in the ansatz. This heuristic construction is based on the fact that, in the short time limit, the system wavefunction $e^{-iHt} |\phi\rangle$ can be exactly described by Eq. 16.

2.4 Engines and Backends

We use the term “engine” to refer to the methods – such as `"tensornetwork"` and `"civector"` – used to simulate the quantum circuits in `TENCIRCHEM`. The term “backend” refers to the underlying numerical package used to perform the simulation, such as `NUMPY` and `JAX`. The most common engine in `TENCIRCHEM` is the `"tensornetwork"` engine powered by `TENSORCIRCUIT`, which views the quantum circuit as a network of low-rank tensors and performs circuit simulation via tensor network contraction.⁷⁶ This approach can offer significant advantages over full statevector simulators which may encounter memory bottlenecks. As a result, tensor network contraction is the most frequently used method for performing large-scale quantum circuit simulations, such as the simulation of random circuits used in quantum supremacy experiments.^{77,78} When contracting a tensor network, it is crucial to find an efficient contraction path. The default contraction path finder in `TENCIRCHEM` is based on a greedy algorithm, which has minimal overhead, but may not be satisfactory for large quantum circuits. The customization of contraction paths is possible via `TENSORCIRCUIT`.

We note that the tensor network contraction simulator should not be confused with an MPS simulator,⁶⁰ although the two do share a number of things in common. In particular, the tensor network contraction method does not assume the circuit wavefunction to adopt MPS form and does not perform any truncations to the wavefunction.

The tensor network simulator can also be extended to the simulation of noisy circuits, using density matrix ρ . The simulation of noisy quantum circuits is thus twice as memory intensive as pure state simulation. We stress that the engine does not perform any truncation to the target density matrix, which is different from a number of preceding works.^{79,80} In the presence of noise, unfortunately, symmetries encoded in the ansatz are broken and cannot be exploited. In `TENSORCIRCUIT`, noise channels \mathcal{E} are defined by their corresponding Kraus

operators K_i , i.e.,

$$\mathcal{E}(\rho) = \sum_i K_i \rho K_i^\dagger. \quad (17)$$

The action of $\{K_i\}$ on the circuit is achieved by transforming them into a superoperator. More specifically, if the channel acts on N qubits, it is converted to a matrix with size $4^N \times 4^N$, as a node in the density matrix tensor network. We note that `TENSORCIRCUIT` supports noisy circuit simulation via Monte-Carlo sampling in addition to using density matrices, although this algorithm is not currently implemented in `TENCIRCHEM`.

Of the various backends supported by `TENCIRCHEM`, the `JAX` backend is perhaps the most versatile and can generally be used in most cases. This backend also supports GPU and TPU calculations once `JAX` is properly configured. If the `"civector"` engine is used, the `NUMPY` and `CUPY` backends are preferred for CPU and GPU calculations, respectively. The reason for this is that the code in the `"civector"` engine is highly optimized and just-in-time (JIT) compilation overheads become a bottleneck.

2.5 Installing and contributing to TenCirChem

`TENCIRCHEM` is written in Python and can be installed via `pip install tencirchem` using the command line. The source code is hosted on the GitHub repository <https://github.com/tencent-quantum-lab/TenCirChem>. We welcome all members of the quantum chemistry community to contribute to the continued development of `TENCIRCHEM`.

3 The Electronic Structure Module I. Unitary-Coupled Cluster ansatz

3.1 Basic Usage

The basic usage of `TENCIRCHEM` can be illustrated in five lines of codes, which we demonstrate below using the UCCSD ansatz to find the minimum energy of an H_2 molecule:

```

1 from tencirchem import M, UCCSD
2
3 h2 = M(atom=[["H", 0, 0, 0], ["H", 0, 0, 0.741]])
4
5 uccsd = UCCSD(h2)
6 uccsd.kernel()
7 uccsd.print_summary(include_circuit=True)

```

Code Snippet 1: Simple UCCSD calculation for the hydrogen molecule.

The remainder of this section will explain Code Snippet 1 in more detail. The corresponding [Jupyter Notebook](#) is available online.

3.1.1 Defining the molecule and basis set

TENCIRCHEM uses the PYSCF `Mole` object to define the molecule of interest. In other words, `from tencirchem import M` is equivalent to `from pyscf import M`. The syntax for defining molecules is thus the same as that for PYSCF. For example, using 3D coordinates, atom types and coordinates (in Angstroms) are specified in a list as shown in Code Snippet 1. By default, the STO-3G minimal basis set is used, but PYSCF allows other basis sets to be specified via the `basis` argument, e.g.,

```

1 h2 = M(atom=[["H", 0, 0, 0], ["H", 0, 0, 0.741]], basis="cc-pvdz")

```

Built-in molecules. In addition to specifying molecules by hand, the user can import a number of pre-specified molecules in STO-3G basis set from the `tencirchem.molecule` module for debugging and fast prototyping, e.g.,

```

1 from tencirchem.molecule import h2, h4, h8

```

Once imported, the molecules can be used exactly as if they had been defined manually. The coordinates and the basis sets of these built-in molecules can be obtained by inspecting the `Mole` object with `m.atom` and `m.basis` respectively. The `tencirchem.molecule.h2` molecule – with a bond distance of 0.741 Å – is frequently used in the following code examples.

3.1.2 Specifying the ansatz and obtaining reference energies

Once the `h2` molecule has been specified, we initialize the UCCSD ansatz via the line

```
1 uccsd = UCCSD(h2)
```

In addition to UCCSD, TENCIRCHEM supports the k -UpCCGSD and pUCCD ansätze. These are based on the UCC base class, and can be implemented in a similar way to UCCSD once imported via:

```
1 from tencirchem import KUPCCGSD, PUCCD
```

Ansatz information is accessible through class attributes (see Code Snippet 2). The conventions for the orbital indices are described in the Supporting Information.

```
1 >>> # two single excitations and one double excitation
2 >>> uccsd.ex_ops
3 [(3, 2), (1, 0), (1, 3, 2, 0)]
4 >>> # 'param_ids' maps excitation operators to parameters
5 >>> # some excitation operators share the same parameter due to symmetry
6 >>> uccsd.param_ids
7 [0, 0, 1]
8 >>> uccsd.init_guess # generated by MP2
9 [0.0, -0.07260814651571333]
10 >>> uccsd.params # the optimized parameters
11 array([ 3.40632986e-17, -1.12995353e-01])
```

Code Snippet 2: Several useful attributes of the UCCSD class. Example corresponds to the H_2 molecule.

UCCSD class as a toolbox. The UCCSD class also allows other useful attributes to be obtained (see Code Snippet 3). The purpose is to make information in TENCIRCHEM easy to inspect, facilitating its use as a handy toolbox. For example, one may use the UCCSD class to inspect for molecular attributes, electron integrals, reference energies and the Jordan-Wigner transformed Hamiltonian, all of which are available without needing to first call the `uccsd.kernel()` method.

```
1 >>> uccsd.n_qubits, uccsd.n_elec
2 (4, 2)
3 >>> # PySCF objects
4 >>> uccsd.mol, uccsd.hf
5 (<pyscf.gto.mole.Mole at 0x7f9daec92b90>, <pyscf.scf.hf.RHF at 0x7f9d92d1ec10>)
6 >>> # reference energies
7 >>> uccsd.e_hf, uccsd.e_mp2, uccsd.e_ccsd, uccsd.e_fci, uccsd.e_nuc
8 (-1.116706137236105,
9 -1.1298675557838804,
10 -1.1372745709766439,
11 -1.1372744055294395,
12 0.7141392859919029)
13 >>> # one and two-body integrals in molecular orbital basis, chemists' notation
14 >>> uccsd.int1e.shape, uccsd.int2e.shape
```

```

15 ((2, 2), (2, 2, 2, 2))
16 >>> uccsd.h_fermion_op # Hamiltonian as openfermion FermionOperator
17 0.7141392859919029 [] +
18 -1.2527052599711868 [0^ 0] +
19 -0.48227117798977825 [0^ 1^ 0 1] +
20 -0.6745650967143663 [0^ 2^ 0 2] +
21 [..... The rest of the output omitted .....]
22 >>> uccsd.h_qubit_op # Hamiltonian as openfermion QubitOperator
23 (-0.09835117053027564+0j) [] +
24 (0.04531660419443148+0j) [X0 X1 X2 X3] +
25 (0.04531660419443148+0j) [X0 X1 Y2 Y3] +
26 (0.04531660419443148+0j) [Y0 Y1 X2 X3] +
27 [..... The rest of the output omitted .....]

```

Code Snippet 3: Several other useful attributes of the UCCSD class are also directly available without first needing to call the `uccsd.kernel()` method.

Specifying integrals directly. Rather than using a molecule as the input to UCCSD, one may define a UCCSD object by specifying the one and two electron integrals, without needing to explicitly refer to a molecule. That is, applying UCCSD to the second-quantized *ab initio* Hamiltonian Eq. 1 can be done via

```

1 uccsd_from_integral = UCCSD.from_integral(int1e, int2e, n_elec, e_core)

```

with

- `int1e`: an array of shape (N, N) with p, q -th element storing the one-electron integral h_{pq} . Here N is the number of spatial orbitals.
- `int2e`: an array of shape (N, N, N, N) with p, q, r, s -th element storing the two-electron integral $(pq|rs)$, in spatial orbital and chemists' notation.
- `n_elec`: an integer specifying the total number of electrons in the system. Currently, TENCIRCHEM only supports closed-shell molecules.
- `e_core`: a floating-point number for the nuclear repulsion energy E_{nuc} or the core energy if frozen occupied orbitals are involved.

3.1.3 Optimizing the energy

The command `uccsd.kernel()` runs the optimization procedure to minimize the ansatz energy with respect to the variational parameters, and returns the minimum energy found.

By default, TENCIRCHEM uses the L-BFGS-B optimizer implemented in SCIPY.⁸¹ Once `uccsd.kernel()` has been run, the minimum ansatz energy can be accessed by `uccsd.energy()` or `uccsd.e_ucc`. The system statevector and configuration interaction vector are available by `uccsd.statevector()` and `uccsd.civector()`, e.g.,

```
1 >>> uccsd.civector() # configuration interaction vector
2 array([ 9.93623806e-01,  1.08284918e-16,  1.08284918e-16, -1.12746318e-01])
```

The optimized parameters can be obtained by `uccsd.params`, and the one- and two-body reduced density matrices are available by `uccsd.make_rdm1()` and `uccsd.make_rdm2()`, respectively. Functions such as `uccsd.energy`, `uccsd.statevector`, and `uccsd.civector` also accept custom circuit variational parameters. For example,

```
1 >>> # if all parameters are zero, then the UCC energy is identical to HF energy
2 >>> uccsd.energy(np.zeros(uccsd.n_params)), uccsd.e_hf
3 (-1.1167061372361045, -1.116706137236105)
```

3.1.4 Outputting quantum circuits

The quantum circuit corresponding to the ansatz state can be obtained via

```
1 c = uccsd.get_circuit()
```

which returns a `TENSORCIRCUIT` circuit object, which can then be inspected, manipulated and executed. For example, a summary of the gates in the circuit can be obtained by

```
1 c.gate_summary()
```

Also, conversion of the circuit from `TENSORCIRCUIT` to Qiskit format is straightforward:

```
1 c_qiskit = c.to_qiskit()
```

By default, TENCIRCHEM compiles circuits using the efficient method of Yordanov, Arvidsson-Shukur, and Barnes (YAB)^{82,83}, which is based on multi-qubit controlled rotations (see Fig. 3). Currently triple or higher order excitations are not implemented in TENCIRCHEM. `uccsd.get_circuit(decompose_multicontrol=True)` generates the circuit with the multi-qubit controlled gate decomposed into elementary rotation gates and CNOT gates. This decomposition is useful for noisy circuit simulation or execution on hardware. See Code Snippet 10 for an example. Compilation via a more traditional Trotterized method is also possible, using

```
1 c = uccsd.get_circuit(trotter=True)
```

although this can lead to circuits significantly deeper than those compiled by the YAB method.⁸²

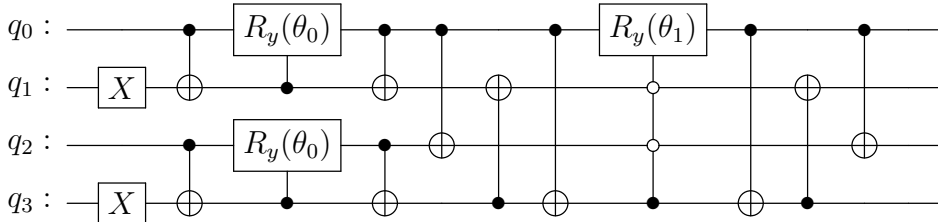


Figure 3: The quantum circuit corresponding to the UCCSD ansatz for the H_2 molecule with STO-3G basis, compiled by the method in Ref. 82. The two X gates at the left of the circuit are used to create the initial Hartree–Fock state $|0101\rangle$. The multicontrol gate applies a parameterized R_y rotation to one of the four qubits, conditioned on the state of the other three.

3.2 Applications and benchmarking

In this section, we use concrete examples to demonstrate the efficiency and flexibility of TENCIRCHEM. All calculations are carried out on a single computational node with the "civector" engine. Throughout the paper, the wall time reported only accounts for VQE optimization time. Classical pre-processings, such as obtaining integrals and Hartree–Fock calculation, are not included in the reported time.

3.2.1 Hydrogen chains and the hydrogen molecule

Table 1 gives the time required by TENCIRCHEM to compute the minimum UCCSD energy for chains of increasing numbers of hydrogen atoms, using an STO-3G basis set. Atoms in each chain are uniformly distributed with an interatomic distance set to 0.8 Å. The largest system simulated is H_{16} , corresponding to 32 qubits. For such a system, storing the wavefunction in Fock space alone is already an arduous task, while the running time for TENCIRCHEM is still acceptable. Whereas other common quantum simulation packages

usually struggle to simulate H_{10} (which requires 20 qubits), TENCIRCHEM is able to obtain the UCCSD ground state energy of this chain in 14 seconds on a single GPU node. As a concrete example, QISKIT-NATURE version 0.5.2 spends 34 seconds simulating H_4 and 943 seconds simulating H_6 , and reports an out-of-memory error when simulating larger systems. Other packages, such as PENNYLANE and TEQUILLA, show similar performance. We note that the high efficiency of TENCIRCHEM is primarily due to the "civector" engine and hardware acceleration plays a relatively minor role.

Table 1: UCCSD ground state energy optimization time for hydrogen chains using TENCIRCHEM. CPU calculations are based on an Intel(R) Xeon(R) Platinum 8255C CPU @ 2.50GHz while GPU calculations use the NVIDIA(R) Tesla(R) V100-PCIE-32GB. Energy errors are with respect to FCI energy, and could be reduced by adding more excitation operators in the ansatz.⁷¹

Molecule	Qubits	Excitations	Parameters	Device	Time (s)	Energy (mH)	Error (mH)
H_4	8	18	11	CPU	0.05	-2,167.55	0.01
H_6	12	69	39	CPU	0.4	-3,204.14	0.27
H_8	16	200	108	CPU	1.9	-4,242.52	0.88
H_{10}	20	467	246	GPU	14	-5,282.21	1.37
H_{12}	24	954	495	GPU	51	-6,322.29	2.13
H_{14}	28	1,749	899	GPU	2,093	-7,362.81	2.92
H_{16}	32	2,976	1,520	GPU	50,909	-8,403.63	3.72

The hydrogen chain actually represents a class of molecular systems that are particularly difficult to simulate in TENCIRCHEM. In these systems, the number of spatial orbitals N is the same as the number of electrons M . In the following, we consider a case at the other extreme, where $M \ll N$, and simulate the potential energy curve of the H_2 molecule using the cc-pVTZ basis set.⁸⁴ This corresponds to $M = 2$, $N = 28$ and a VQE circuit on 56 qubits. Running on a single laptop CPU, TENCIRCHEM is able to produce all UCCSD energy values in Table 2 in 20 seconds. Because of the small value of M , both the dimension of the configuration interaction space (784) and the number of excitation operators (155) are small. Since the "civector" engine is exact, the small error in Table 2 is likely due to the inexactness of the disentangled UCC ansatz.

Table 2: UCCSD/cc-pVTZ calculation of H_2 in TENCIRCHEM, using a VQE circuit on 56 qubits. Energy errors are with respect to FCI.

Atom distance (Å)	Energy(mH)	Error (mH)
0.3	-692.85983	0.00000
0.6	-1153.51794	0.00000
0.9	-1160.41280	0.00001
1.2	-1112.06753	0.00005
1.5	-1066.16823	0.00014
1.8	-1034.07993	0.00023
2.1	-1015.56097	0.00028
2.4	-1006.42068	0.00029
2.7	-1002.39048	0.00028

3.2.2 Potential energy curve of H_2O

We now compute the potential energy curve of a realistic molecule, H_2O . The [Python script](#) to produce the data is available online. This molecule has been used to benchmark many quantum algorithms,^{85,86} yet previous works usually use a minimal basis set or small active space. Here, we use TENCIRCHEM to calculate the UCCSD energy of H_2O with 6-31G(d) basis set^{87,88} with only the 1s orbital of the O atom frozen. This corresponds to 8 electrons in 17 orbitals, a quantum circuit on 34 qubits, and an ansatz involving 565 independent parameters and 1078 excitations.

We study the symmetric stretching of the O-H bond with the H-O-H angle fixed at the experimental value of 104.45° .⁸⁹ Results are summarized in Fig. 4. The UCCSD energy by TENCIRCHEM is very close to the FCI solution with a slight deviation observed at long bond lengths. The equilibrium bond length is determined to be 0.97 Å, in good agreement with the experimental value (0.9584 Å). To highlight the necessity of using an appropriate basis set, in Fig. 4 the FCI energy using the minimal STO-3G basis set is also given. As expected, the energy corresponding to the STO-3G basis set is significantly higher than that corresponding to the 6-31G(d) basis set. Furthermore, the equilibrium bond distance predicted using the STO-3G basis set is 1.02 Å, significantly larger than the experimental value. On average, TENCIRCHEM takes approximately 15 minutes to produce each UCCSD

energy value in Fig. 4, using the same GPU platform as in Table 1.

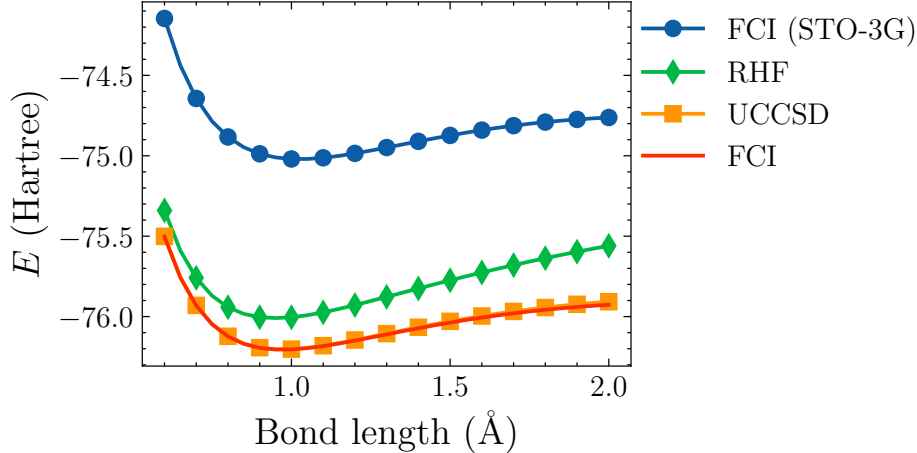


Figure 4: Potential energy curve for the symmetric stretching of the O-H bond in H_2O with 6-31G(d) basis set. The $1s$ orbital of the O atom is frozen and the whole system is described by an (8e, 17o) active space and a quantum circuit on 34 qubits. The FCI energy with STO-3G basis set is included for comparison.

3.2.3 Hubbard model

As a final example, we use TENCIRCHEM and UCCSD to calculate the ground state energy of the one-dimensional Hubbard model at half-filling. The full [Jupyter Notebook](#) is available online. The Hamiltonian is

$$H = -t \sum_{j,\sigma} (c_{j+1,\sigma}^\dagger c_{j,\sigma} + c_{j,\sigma}^\dagger c_{j+1,\sigma}) + U \sum_j n_{j\uparrow} n_{j\downarrow}, \quad (18)$$

where $c_{j,\sigma}^\dagger$ ($c_{j,\sigma}$) creates (annihilates) an electron with spin σ at site j , $n_{j\uparrow}$ and $n_{j\downarrow}$ are electron occupation number operators at site j , t is the hopping integral and U characterizes the Coulomb repulsion interaction strength. We assume periodic boundary conditions.

Although the Hubbard model is not directly related to any molecular systems, the Hamiltonian is a special case of the *ab initio* Hamiltonian of Eq. 1, and thus TENCIRCHEM allows the construction of the corresponding UCCSD objects by specifying the one-body and two-body integrals.

```

1 import numpy as np
2 from tencirchem import UCCSD
3
4 n = 6 # the number of sites
5 n_elec = n # half filled
6 t = U = 1 # model parameters
7
8 # setup the integrals
9 int1e = np.zeros((n,n))
10 for i in range(n - 1):
11     int1e[i, i + 1] = int1e[i + 1, i] = -t
12 int1e[n - 1, 0] = int1e[0, n - 1] = -t
13 int2e = np.zeros((n, n, n, n))
14 for i in range(n):
15     int2e[i, i, i, i] = U
16
17 # do the calculation
18 uccsd = UCCSD.from_integral(int1e, int2e, n_elec)
19 uccsd.kernel()

```

Code Snippet 4: Calculation of the UCCSD energy of half-filled Hubbard model.

Results are shown in Fig. 5. When U/t is small, both CCSD and UCCSD coincide well with the FCI solution. As U/t increases, CCSD deviates from the FCI solution, whereas the UCCSD solution tracks the FCI value much more closely, indicating that UCCSD can be better than CCSD at capturing strong correlations, a finding consistent with a previous report.⁹⁰

To better recover static correlation using UCCSD, more terms can be added to the UCC ansatz or one may consider combining UCC with other algorithms, such as density matrix embedding theory.^{47,91–94} On average, TENCIRCHEM requires 0.1 seconds to calculate each UCCSD energy value in Fig. 5 on a regular CPU without GPU acceleration.

4 The Electronic Structure Module II. Hardware-efficient Ansatz and Noisy Circuit Simulation

In real-world quantum computing systems, noise and errors are inevitable due to factors such as imperfect hardware, decoherence, and finite-shot measurement uncertainty. Noisy circuit simulators allow researchers to simulate the effects of noise on quantum circuits and get a better understanding of the behavior of quantum algorithms in realistic conditions. In this

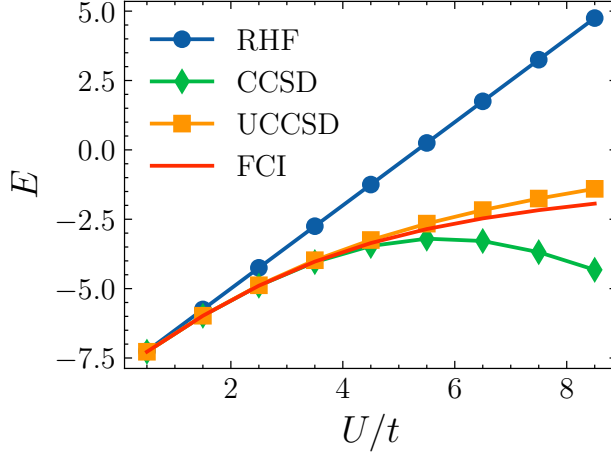


Figure 5: Ground state energy of one-dimensional half-filled Hubbard model by UCCSD with increasing coulomb repulsion strength U/t . The UCCSD energy computed by TENCIRCHEM tracks the FCI value significantly better than CCSD does.

section, we use the hydrogen molecule H_2 to illustrate how to perform noisy circuit simulation in TENCIRCHEM. After using the parity transformation, the corresponding Hamiltonian acts on 2 qubits. The [Jupyter Notebook](#) for this section is available online.

4.1 Basis Usage

TENCIRCHEM uses the HEA (Hardware-Efficient Ansatz) class for noisy circuit simulation, which has a different interface from the UCC classes encountered in Sec. 3. A primary motivation for using HEA ansätze is that almost all UCC circuits (with perhaps pUCCD circuits being the exception) are too large for both noisy circuit simulation as well as execution on currently available quantum devices. In contrast, HEA circuits are, by design, constructed to be implementable on whatever device is available.

Another reason is that, from a user’s perspective, the HEA class ought to provide a greater degree of low-level customization compared to the UCC classes. For example, for noiseless UCC simulation, the ansatz is defined by excitation operators and compilation to native gates is of less interest. Conversely, in the context of noisy HEA circuit simulation, it is imperative to give users complete control over the ansatz circuit. Nevertheless, noisy UCC

circuit simulation can be carried out within TENCIRCHEM without much additional effort, which will be demonstrated in Sec. 4.1.3.

4.1.1 Specifying the Hamiltonian and the ansatz

Unlike UCC, the HEA class is not initialized by specifying the molecule. Rather, HEA takes as inputs (i) the Hamiltonian in `openfermion.QubitOperator` form and (ii) the circuit ansatz.

Within OPENFERMION, the Hamiltonian can be constructed by interfacing with quantum chemistry packages, such as PYSCF using `openfermion.MolecularData`.

```
1 from openfermion import MolecularData
2 from openfermionpyscf import run_pyscf
3
4 geometry = [["H", [0, 0, 0]], ['H', [0, 0, 0.741]]]
5 basis = "STO-3G"
6 multiplicity = 1
7 molecule = MolecularData(geometry, basis, multiplicity)
8 molecule = run_pyscf(molecule)
9 h_fermion_op = molecule.get_molecular_hamiltonian()
```

Code Snippet 5: Construction of the system Hamiltonian in fermion operator form using OPENFERMION.

An alternative approach is to use the UCC class attributes, such as `uccsd.h_fermion_op`.

```
1 from tencirchem import UCCSD, parity
2 from tencirchem.molecule import h2
3
4 uccsd = UCCSD(h2)
5 # Hamiltonian as openfermion.FermionOperator
6 h_fermion_op = uccsd.h_fermion_op
7 # use parity transformation for qubit Hamiltonian and remove 2 qubits
8 h_qubit_op = parity(h_fermion_op, uccsd.n_qubits, uccsd.n_elec)
```

Code Snippet 6: Construction of the system Hamiltonian in qubit operator form using UCCSD class attributes.

The ansatz is defined using TENSORCIRCUIT. In the example below, we construct a 1-layer R_y ansatz comprising 4 parameters and the circuit diagram is depicted in Fig. 6. The initial parameters create the HF state $|01\rangle$ under parity transformation. In addition to defining the ansatz from scratch, it is also possible to use a pre-defined ansatz, which will be discussed more thoroughly in Sec. 4.1.3.

```
1 import numpy as np
2 from tensorcircuit import Circuit
3
4 n_qubits = 2
```

```

5 n_params = 4
6 init_guess = [0, np.pi, 0, 0]
7 def get_circuit(params):
8     c = Circuit(n_qubits)
9     # the ansatz body
10    c.ry(0, theta=params[0])
11    c.ry(1, theta=params[1])
12    c.cnot(0, 1)
13    c.ry(0, theta=params[2])
14    c.ry(1, theta=params[3])
15    return c

```

Code Snippet 7: Defining the 1-layer R_y ansatz using TENSORCIRCUIT.

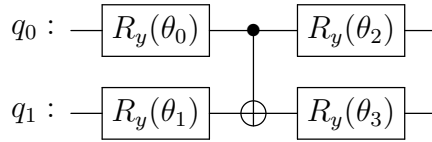


Figure 6: Circuit diagram for a 2-qubit 1-layered R_y ansatz. More layers can be added by repeating the CNOT and R_y rotation unit.

4.1.2 Noisy circuit simulation and optimization

The remaining workflow is similar to the UCCSD case: (i) create an HEA instance, (ii) run the kernel, and (iii) print the summary:

```

1 from tencircchem import HEA
2 hea = HEA(h_qubit_op, get_circuit, init_guess, engine="tensornetwork-noise")
3 hea.kernel()
4 hea.print_summary()

```

The default optimizer used is again L-BFGS-B from SciPy.

The gradients are evaluated by the parameter-shift rule.^{32,33} The parameter-shift rule uses two separate circuits to evaluate the gradient of one parameter. Its essence can be summarized using a single-qubit single-gate illustrative example. Suppose the circuit wavefunction is $|\psi\rangle = e^{\theta R}|\phi\rangle$ with $R^2 = -I$. This leads to $|\psi\rangle = (\cos\theta + \sin\theta R)|\phi\rangle$, and the energy expectation is then

$$\langle E \rangle(\theta) = \cos^2\theta \langle \phi | H | \phi \rangle + \sin\theta \cos\theta \langle \phi | RH + HR | \phi \rangle + \sin^2\theta \langle \phi | RHR | \phi \rangle . \quad (19)$$

Thus

$$\frac{\partial \langle E \rangle}{\partial \theta} = \langle E \rangle \left(\theta + \frac{\pi}{4} \right) - \langle E \rangle \left(\theta - \frac{\pi}{4} \right). \quad (20)$$

The expression is slightly different from the literature where $e^{\frac{\theta}{2}R}$ is usually assumed.

By default, using the "tensornetwork-noise" engine (line 2) adds isotropic depolarizing noise⁹⁵ with error probability $p = 0.02$

$$\mathcal{E}(\rho) = (1 - p)\rho + \frac{p}{15} \sum_{j=1}^{15} \mathcal{P}_j \rho \mathcal{P}_j. \quad (21)$$

to each CNOT gate in the circuit. Here ρ is the density matrix, and the \mathcal{P}_j are the two-qubit Pauli matrices (excluding the identity operator I). Hereafter we will also refer to p as the CNOT error probability. The value $p = 0.02$ corresponds to approximately 98% CNOT average gate fidelity, defined as

$$F = \int \langle \psi | \mathcal{E}(|\psi\rangle \langle \psi|) | \psi \rangle d\psi = 1 - \frac{4}{5}p. \quad (22)$$

Single qubit gate noise is not included. The energy obtained in this case is -1.1203.

Other noise models can be specified using the `NoiseConf` class from `TENSORCIRCUIT`, as illustrated below:

```
1 from tensorcircuit.noisemodel import NoiseConf
2 from tensorcircuit.channels import isotropicdepolarizingchannel
3
4 engine_conf = NoiseConf()
5 # larger noise, corresponding to 80%
6 channel = isotropicdepolarizingchannel(p=0.25, num_qubits=2)
7 engine_conf.add_noise("cnot", channel)
8
9 hea = HEA(h_qubit_op, get_circuit, init_guess, \
10          engine="tensornetwork-noise", engine_conf=engine_conf)
11 hea.kernel()
12 hea.print_summary()
```

Code Snippet 8: A simple customized noise model with depolarizing error probability $p = 0.25$, corresponding to average gate fidelity of 80%. The energy obtained is -0.9245, higher than the value of -1.1203 obtained from the $p = 0.02$ case.

In addition to the depolarizing channel, `TENSORCIRCUIT` supports the amplitude damping channel, phase damping channel, and thermal relaxation channel.⁹⁵

The "tensornetwork-noise" engine does not consider measurement uncertainty. Measurement uncertainty can be accounted for using the "tensornetwork-noise&shot" engine, as shown below:

```

1 >>> # number of shots: 4096
2 >>> for i in range(5):
3 >>>     print(hea.energy(engine="tensornetwork-noise&shot"))
4 -0.9209869918508058
5 -0.9306141224500795
6 -0.9176478740443613
7 -0.929275708950061
8 -0.9241459510180587
9 >>> # number of shots: 4096 * 128
10 >>> hea.shots = 4096 * 128
11 >>> for i in range(5):
12 >>>     print(hea.energy(engine="tensornetwork-noise&shot"))
13 -0.9246797253478469
14 -0.9251027083245665
15 -0.9243841547125008
16 -0.9236478492038139
17 -0.9248303187894168

```

Code Snippet 9: Accounting for measurement uncertainty in noisy circuit simulation using the "tensornetwork-noise&shot" engine.

By default, the number of measurement shots made for each term in the Hamiltonian is 4096. Increasing the number of measurement shots decreases the energy uncertainty. Here the engine is switched temporarily at runtime, and specifying the engine while initializing the HEA class is also viable, by `hea=HEA(*args, engine=engine)`.

If desired, a real quantum hardware engine can be specified by setting the engine to "qpu". The circuit is then executed on a 9-qubit super-conducting QPU hosted by the Tencent Quantum Lab quantum cloud service. A private token is required for successful execution. The platform is currently under closed beta and we are developing more features. The access token and configuration documents can be requested by sending an email to the authors.

If noiseless results are desired for the HEA ansatz, this can be achieved by using the "tensornetwork" engine, i.e., `hea.energy(engine="tensornetwork")`. In this case, the energy is in exact agreement with the FCI energy for the hydrogen molecule system.

4.1.3 Using pre-defined ansätze

At the end of the section, we show how to use pre-defined ansätze for noisy circuit simulation. TenCirChem has implemented the R_y ansatz. In the following code the HEA instance is rebuilt using the HEA.ry function, which constructs the qubit Hamiltonian and the R_y ansatz automatically. The result after running the kernel is exactly the same as what we've illustrated step by step above.

```
1 hea = HEA.ry(uccsd.int1e, uccsd.int2e, uccsd.n_elec, uccsd.e_core, \
2             n_layers=1, engine="tensornetwork-noise")
3 hea.kernel()
```

If desired, the UCC ansatz defined in the UCC class can be fed into the HEA class for noisy circuit simulation. The following code snippet shows how to simulate the UCCSD circuit of the H_2 molecule in the presence of noise. As described in Sec. 3.1.4, TENCIRCHEM by default uses a multi-qubit controlled R_y gate for UCC circuit simulation, which has to be decomposed into elementary gates before actual execution on quantum computers. The gradient is turned off because the parameter-shift rule is not directly applicable to the circuit in which multiple gates share the same parameter. The COBYLA optimizer implemented in SciPy⁸¹ is used for optimization. The energy obtained is -0.8358, which is significantly higher than the energy by the HEA ansatz, because there are 18 noisy CNOT gates in the circuit. We comment that simulating UCC circuits with the HEA class is non-standard. Usually, it is necessary to simplify the ansatz before execution under realistic hardware conditions.^{11,12}

```
1 from functools import partial
2 get_circuit = partial(uccsd.get_circuit, decompose_multicontrol=True)
3 hea = HEA(uccsd.h_qubit_op, get_circuit, uccsd.init_guess, \
4          engine="tensornetwork-noise")
5 hea.grad = "free"
6 hea.kernel()
```

Code Snippet 10: Noisy simulation of UCC circuits.

4.2 Applications

4.2.1 Effect of gate noise on VQE energy

As a first application, we show how the CNOT depolarizing error affects the optimized VQE energy. Results are shown in Fig. 7. The R_y hardware-efficient ansatz and the H_2 molecule with parity transformation are used, as in Sec. 4.1.

We additionally test how the number of ansatz layers affects the obtained energy. If a one-layer ansatz is adopted, the energy increases linearly with the error probability up to $p = 0.8$. This is a consequence of the fact that this ansatz, when compiled into a quantum circuit, contains only a single CNOT gate. Increasing the number of layers does not lead to more accurate energy estimation. Rather, the noise caused by more CNOT gates in the ansatz further degrades the results. TENCIRCHEM requires approximately 1 second to produce each data point in Fig. 7, which involves iterating the VQE parameter optimization procedure until convergence.

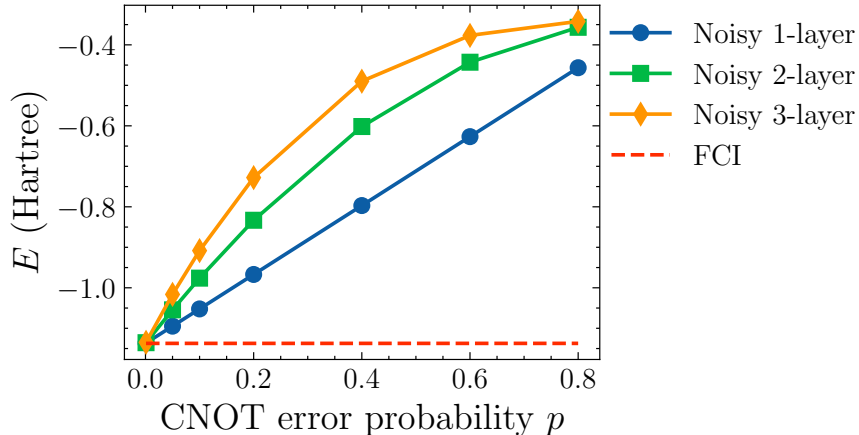


Figure 7: The VQE ground state energy of H_2 with parity transformation in the presence of depolarizing error, characterized by the error probability p . The R_y hardware-efficient ansatz is used, with between 1 and 3 layers.

4.2.2 Effect of measurement shots on VQE energy uncertainty

Here we show how the number of measurement shots N_{shots} affects the standard deviation of the optimized VQE energy. Results are shown in Fig 8. The H_2 molecule of Sec. 4.2.1 is used with a single layer R_y ansatz. We test N_{shots} values from 2^8 to 2^{13} . For each value of N_{shots} investigated, the system energy E is evaluated 64 times and the standard deviation is calculated. Note that the circuit parameters are kept constant at the optimal value and the VQE iteration is not run.

As expected, the standard deviation of E is proportional to $\sqrt{\frac{1}{N_{\text{shots}}}}$.¹ Increasing the error probability p causes a larger standard deviation of the energy, although the effect is far less significant than that caused by adjusting N_{shots} . TENCIRCHEM requires approximately 1 second to produce a single data point in Fig. 8, each of which involves 64 separate energy evaluations.

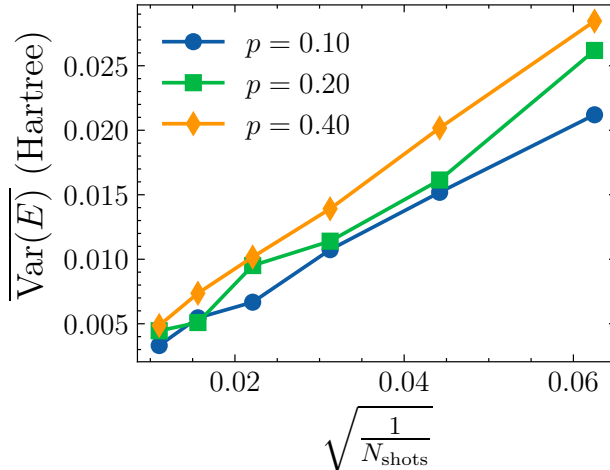


Figure 8: The VQE energy in the presence of depolarizing error, characterized by the error probability p . The R_y circuit with 1 layer is used as the ansatz.

4.2.3 Running quantum hardware experiments

In this section, we use QPUs to compute the VQE energy of the H_2 molecule, and the results are summarized in Fig. 9. We use the same one-layered R_y ansatz described in previous sections. To reduce the computational cost, the parameter vector is reduced to $[\theta, \pi, 0, 0]$

with only one variable θ . Noiseless simulation shows that using this ansatz is sufficient to reach the FCI energy. On QPU, 8192 shots are taken to determine the expectation value of each term in the Hamiltonian. The error is mitigated by standard readout error mitigation. For each set of circuit parameters, the energy is evaluated 8 times to produce the final energy expectation and its standard deviation. We first compute the potential energy curve using the classically optimized parameter and then run the full VQE optimization starting from $\theta = 0$. In both cases, the QPU engine can correctly describe the dissociation curve of the H_2 molecule. Moreover, we observe that the energy standard deviation increases as the bond length decreases. This is because at short bond lengths the Pauli strings have large coefficients due to strong interaction between the particles.

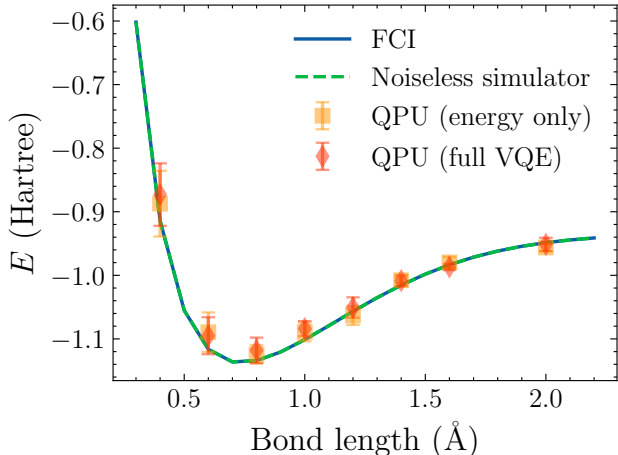


Figure 9: The VQE potential energy curve of H_2 computed on a QPU backend. QPU energies obtained from the classically optimized parameter and full VQE optimization process are both shown.

5 The Quantum Dynamics Module

5.1 Basic Usage

5.1.1 Defining the Hamiltonian and basis set

The first step in quantum dynamics simulations is specifying the Hamiltonian. In this section, we focus on the spin-boson model with 1 bosonic mode:

$$H = \frac{\epsilon}{2}\sigma_z + \Delta\sigma_x + \omega b^\dagger b + g\sigma_z(b^\dagger + b) \quad (23)$$

where $\sigma_z = Z$ and $\sigma_x = X$ are Pauli matrices, ϵ is the eigenfrequency and Δ is the tunnelling rate. The spin-boson model is a classical model for a variety of chemical processes, such as electron transfer and photochemistry.⁹⁶ For ease of demonstration, we truncate the allowed boson states to two levels. More sophisticated examples can be found in Sec. 5.3 and in the online [Jupyter Notebook](#).

Defining the system Hamiltonian and basis sets is performed as follows:

```
1 from tencirchem import Op, BasisHalfSpin, BasisSHO
2
3 epsilon = 0
4 delta = 1
5 omega = 1
6 g = 0.5
7
8 ham_terms = [
9     Op("sigma_z", "spin", epsilon),
10    Op("sigma_x", "spin", delta),
11    Op(r"b^\dagger b", "boson", omega),
12    Op("sigma_z", "spin", g) * Op(r"b^\dagger+b", "boson")
13 ]
14 basis = [BasisHalfSpin("spin"), BasisSHO("boson", omega=omega, nbas=2)]
```

Code Snippet 11: Defining the system Hamiltonian and basis set for 1-mode spin-boson model.

The `Op` and the basis set classes are directly imported from the `RENORMALIZER` package. Each term in the Hamiltonian takes three arguments: (i) the operator symbol; (ii) the name of the associated degree of freedom; and (iii) the (optional) coefficient.

In setting the basis sets (line 14), `BasisSHO` refers to the simple harmonic oscillator basis,

and `nbas=2` restricts the phonon states to the lowest two levels.

Conversion of the Hamiltonian and basis sets into qubits is then performed in TENCIRCHEM using the `qubit_encode_op` and `qubit_encode_basis` commands, as illustrated below:

```
1 from tencirchem.dynamic import qubit_encode_op, qubit_encode_basis
2 boson_encoding = "gray"
3 ham_terms_spin, constant = qubit_encode_op(ham_terms, basis, boson_encoding)
4 basis_spin = qubit_encode_basis(basis, boson_encoding)
```

Code Snippet 12: Transformation from physical basis set into qubit spin basis. Here we use the binary encoding with Gray code approach (see Sec. 2.2.2) to encode the bosonic states.

After transformation, the Hamiltonian and basis sets can be inspected as follows:

```
1 >>> ham_terms_spin
2 [Op('X', ['spin'], 1.0),
3  Op('Z', [('boson', 'TCCQUBIT-0')], -0.5),
4  Op('Z X', ['spin', ('boson', 'TCCQUBIT-0')], 0.5)]
5 >>> basis_spin
6 [BasisHalfSpin(dof: spin, nbas: 2),
7  BasisHalfSpin(dof: ('boson', 'TCCQUBIT-0'), nbas: 2)]
```

Code Snippet 13: Inspection of the transformed Hamiltonian.

As expected, the Hamiltonian is now expressed in terms of Pauli strings and the basis sets are all transformed to the spin- $\frac{1}{2}$ basis set. Here, the term in square brackets in each operator of the above Code Snippet represents the label(s) of the spin- $\frac{1}{2}$ basis on which the Pauli operators are defined. As we restrict to two phonon levels, only one spin- $\frac{1}{2}$ basis set with label `('boson', 'TCCQUBIT-0')` is generated, i.e., the phonon mode is represented by a single qubit.

5.1.2 Construct the ansatz

The variational Hamiltonian ansatz (see Fig. 10) defined in Eq. 16 can now be constructed using the `get_ansatz` function, and the Jacobian then obtained by `get_jacobian_func`:

```
1 import tensorcircuit as tc
2 from tencirchem import set_backend
3 from tencirchem.dynamic import get_ansatz, get_jacobian_func
4
5 # dynamics simulation requires auto-differentiation from JAX.
6 set_backend("jax")
7
8 # the initial state
9 init_circuit = tc.Circuit(len(basis_spin))
```

```

10 # number of layers
11 n_layers = 3
12 # get the ansatz. Note that the spin basis is fed in
13 ansatz = get_ansatz(ham_terms_spin, basis_spin, n_layers, init_circuit)
14
15 # ansatz accepts parameters and outputs wavefunction
16 import numpy as np
17 print(ansatz(np.zeros(n_layers * len(ham_terms_spin))))
18 # the function to evaluate the jacobian of the wavefunction
19 jacobian_func = get_jacobian_func(ansatz)

```

Code Snippet 14: Construction of the ansatz and the function to evaluate the Jacobian.

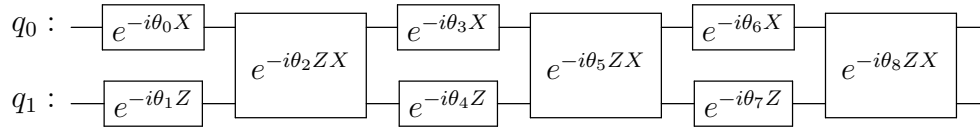


Figure 10: Quantum circuit corresponding to the 3-layered variational Hamiltonian ansatz for the 1-mode spin-boson model using binary encoding with Gray code. q_0 represents the spin and q_1 represents the boson.

Here, `basis_spin` defines the ordering of the qubits in the circuit. More specifically, the first and second elements in `basis_spin` refer to the spin and boson respectively, and thus in the quantum circuit the first qubit represents the spin and the second qubit represents the boson. Note that the backend needs to be set to JAX explicitly because the default NUMPY backend does not support automatic differentiation.

5.1.3 Time evolution

With the ansatz function to calculate the wavefunction and its Jacobian, the equation of motion Eq. 5 can now be readily solved to determine $\dot{\theta}_k$. The following code wraps the derivative function in SCIPY format and solves the initial value problem. The wavefunction is evolved from time $t = 0$ to $t = 10$ using a time interval of 0.1.

```

1 from tencirchem import get_dense_operator
2 from tencirchem.dynamic import get_deriv
3 # the Hamiltonian in dense matrix format
4 h = get_dense_operator(basis_spin, ham_terms_spin)
5 # time derivative for circuit parameters in the scipy solve_ivp format
6 def scipy_deriv(t, _theta):
7     return get_deriv(ansatz, jacobian_func, _theta, h)

```

```

8 from scipy.integrate import solve_ivp
9 # time step
10 tau = 0.1
11 # initial value
12 theta = np.zeros(n_layers * len(ham_terms_spin))
13 for n in range(100):
14     # time evolution
15     scipy_sol = solve_ivp(scipy_deriv, [n * tau, (n + 1) * tau], theta)
16     # time evolved parameter
17     theta = scipy_sol.y[:, -1]

```

Code Snippet 15: Time evolution of the spin-boson system.

Note that TENCIRCHEM also provides a high-level interface for simulating dynamics,

e.g.,

```

1 from tencirchem import TimeEvolution
2
3 te = TimeEvolution(ham_terms, basis)
4 for i in range(100):
5     te.kernel(0.1)

```

Code Snippet 16: Time evolution of the spin-boson system using the `TimeEvolution` class.

Using this interface, the user need only specify the Hamiltonian and the basis sets, and encoding to qubits is carried out automatically using binary encoding with Gray code. Configuration of the encoding strategy, the circuit initial condition, and the number of layers in the ansatz are also supported.

5.2 Implementation

TENCIRCHEM uses classical matrix manipulations to calculate the M matrix and V vector in the equation of motion (Eq. 4) instead of faithfully simulating the quantum circuit. The first step is to obtain the Jacobian $\frac{\partial |\Psi\rangle}{\partial \theta_k}$ by forward-mode auto-differentiation via the JAX backend. Forward-mode auto-differentiation is preferred over reverse-mode auto-differentiation in this case, because usually there are more amplitudes in $|\Psi\rangle$ than parameters θ_k . The whole matrix M is then calculated by a single matrix-matrix multiplication according to Eq. 5. Similarly, the whole vector V is calculated by computing $H|\psi\rangle$ via a single matrix-vector multiplication, and then another matrix-vector multiplication between the Jacobian and $H|\psi\rangle$. This implementation minimizes the just-in-time compile time in JAX, because evaluating the Jacobian is the only bottleneck that needs to be compiled during the workflow.

The M matrix is usually not invertible due to linear dependencies in $\frac{\partial|\Psi\rangle}{\partial\theta_k}$. Its eigenvalues λ_i are modified with $\lambda_i \rightarrow \lambda_i + \epsilon e^{-\lambda_i/\epsilon}$ for regularization, where ϵ is a pre-defined small number, typically 1×10^{-5} .

5.3 Applications

5.3.1 Spin relaxation of spin-boson model

Here we show the simulated dynamics of the 1-mode spin-boson model defined in Eq. 23, with parameters $\epsilon = 0$, $\Delta = 1$, $\omega = 1$ and $g = 0.5$. Unlike the previous example which truncated the boson to the lowest two states, here we allow 8 bosonic states, and the corresponding circuit acts on 4 qubits. The simulated results are shown in Fig. 11, and are in good agreement with the solution with exact diagonalization.

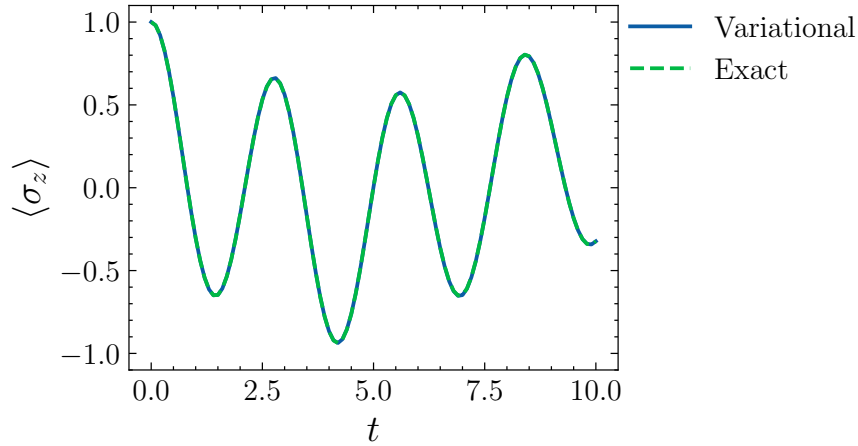


Figure 11: Spin relaxation of the 1-mode spin-boson model simulated by variational quantum dynamics.

5.3.2 Marcus inverted region of the charge transfer model

In this section, we simulate the charge transfer or oxidation-reduction reaction between two molecules using the Marcus model⁹⁷

$$H = -V(a_0^\dagger a_1 + a_1^\dagger a_0) + \Delta G a_1^\dagger a_1 + \omega \sum_{i=0,1} b_i^\dagger b_i + g\omega \sum_{i=0,1} a_i^\dagger a_i (b_i^\dagger + b_i). \quad (24)$$

Here a_0 and a_1 are annihilation operators for the charge on the first and the second molecule respectively. We assume transfer integral $V = -0.1$, dimensionless coupling constant $g = 1$, and vibration frequency $\omega = 0.5$. The Marcus charge transfer theory predicts that, by decreasing the reaction Gibbs free energy change ΔG , the reaction rate k will first increase and then decrease, according to

$$k = \frac{V^2}{\hbar} \sqrt{\frac{\pi\beta}{\lambda}} \exp\left\{-\frac{\beta(\lambda + \Delta G)^2}{4\lambda}\right\} \quad (25)$$

where $\lambda = 2g^2\omega$ is the reorganization energy and β is the inverse temperature. Due to the quadratic term on the exponential, the maximum rate is reached when $\Delta G = -\lambda = -1$.

In the simulation, we again truncate the number of boson states to 8, and thus the Hamiltonian is encoded into 7 qubits using the Gray code method. The charge is initially set to be located at the first molecule and the nuclear coordinates are relaxed according to the localized charge.⁹⁸ The system is then evolved to $t = 8$ using TENCIRCHEM and we compute $\langle a_0^\dagger a_0 \rangle$ (the charge occupation on the first molecule) as a function of time, with ΔG ranging from 0 to -2. The full [Jupyter Notebook](#) is available online.

Results are shown in Fig. 12(a). During an initial period ($t < 2$), the reaction rate increases with t . For $2 < t < 8$, the reaction reaches a steady state and the reaction rate is approximately constant.

In Fig. 12(b) we plot the reaction rate k from $t = 2$ to $t = 8$. Since the effect of temperature is not modeled in this simulation, β is fit to a value of 2.71 by matching the simulated $k(\Delta G)$ data with the least square method. The simulated rate reaches the maximum at $\Delta G = -1$, in agreement with the theoretical prediction. We also include the charge transfer rate from full quantum nuclear tunneling enabled charge transfer theory,⁹⁹ which predicts a very similar parabolic curve without fitting β .

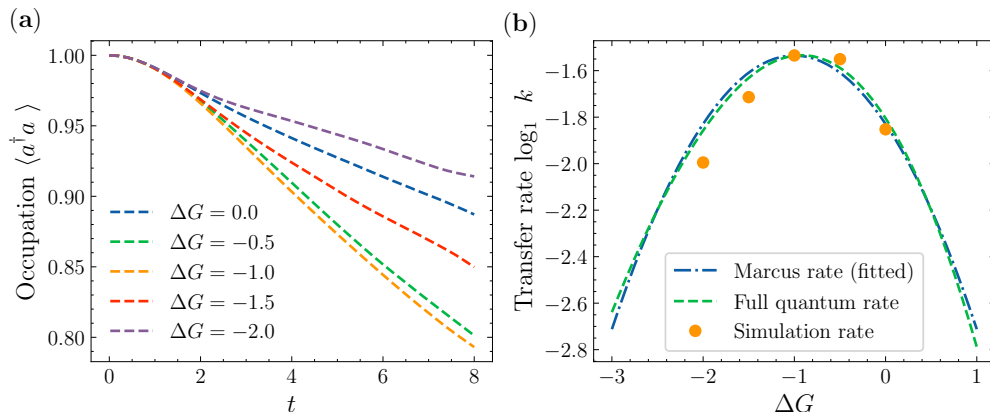


Figure 12: (a) Charge occupation on the first molecule versus time at several values of ΔG . (b) Charge transfer rate k as a function of ΔG , for $2 < t < 8$. The dots are from a linear fit based on $\langle a_0^\dagger a_0 \rangle(t) = -kt + c$ to the linear region in (a) and the dashed lines are the predictions of the Marcus theory (Eq. 25) and full quantum charge transfer theory.

6 Summary and Outlook

In this paper, we introduce TENCIRCHEM, a Python-based open-source library for quantum computational chemistry, hosted on the GitHub repository <https://github.com/tencent-quantum-lab/TenCirChem>. TENCIRCHEM aims to provide both black-box calculations of existing quantum algorithms and flexible interfaces for rapid prototyping of novel computational methods. TENCIRCHEM features high-performance UCC calculations, noisy circuit simulation with both quantum gate error and measurement noise, and variational quantum dynamics simulation. TENCIRCHEM is designed to expose its internal data structure for inspection and modification, enabling in-depth customization. Although written in Python, TENCIRCHEM reaches state-of-the-art performance via the powerful TENSORCIRCUIT backend and various chemistry-focused optimizations, such as UCC factor expansion. Its efficiency is demonstrated by the exact UCCSD simulation of H_{16} in STO-3G basis (32 qubits), H_2 in cc-pVTZ basis (56 qubits), and H_2O in 6-31G(d) basis (34 qubits), requiring only moderate computational time and hardware.

The development of TENCIRCHEM is an ongoing process. In the future, additional QPU engine configuration options will be provided. Features such as support for higher

order excitations, the treatment of open-shell systems, algorithms for excited states and periodic systems, algorithms for fault-tolerant quantum computers, further performance optimization, and more code examples reproducing published algorithms are also under active consideration.

Acknowledgement

The authors thank Zhaofeng Ye for designing the TENCIRCHEM logo. Weitang Li would like to thank Sainan Huai and Tianqi Cai for their helpful discussions. This work is supported by the National Natural Science Foundation of China through grant numbers 22273005 and 21788102. This work is also supported by Shenzhen Science and Technology Program.

Supporting Information

The Supporting Information is available free of charge online, including

- A brief review of UCC ansätze implemented in TENCIRCHEM.
- The conventions for orbital indices and qubit indices in TENCIRCHEM.
- The output of the `print_summary` command.
- Advanced features of the UCC classes.
- The algorithm for efficient simulation of UCC circuits.

References

- (1) McClean, J. R.; Romero, J.; Babbush, R.; Aspuru-Guzik, A. The theory of variational hybrid quantum-classical algorithms. *New J. Phys.* **2016**, *18*, 023023.
- (2) Cao, Y.; Romero, J.; Olson, J. P.; Degroote, M.; Johnson, P. D.; Kieferová, M.; Kivlichan, I. D.; Menke, T.; Peropadre, B.; Sawaya, N. P.; Sim, S.; Veis, L.; Aspuru-

- Guzik, A. Quantum chemistry in the age of quantum computing. *Chem. Rev.* **2019**, *119*, 10856–10915.
- (3) Bauer, B.; Bravyi, S.; Motta, M.; Chan, G. K.-L. Quantum algorithms for quantum chemistry and quantum materials science. *Chem. Rev.* **2020**, *120*, 12685–12717.
- (4) McArdle, S.; Endo, S.; Aspuru-Guzik, A.; Benjamin, S. C.; Yuan, X. Quantum computational chemistry. *Rev. Mod. Phys.* **2020**, *92*, 015003.
- (5) Liu, J.; Fan, Y.; Li, Z.; Yang, J. Quantum algorithms for electronic structures: basis sets and boundary conditions. *Chem. Soc. Rev.* **2022**,
- (6) Preskill, J. Quantum Computing in the NISQ era and beyond. *Quantum* **2018**, *2*, 79.
- (7) Arute, F.; Arya, K.; Babbush, R.; Bacon, D.; Bardin, J. C.; Barends, R.; Biswas, R.; Boixo, S.; Brandao, F. G. S. L.; Buell, D. A.; Burkett, B.; Chen, Y.; Chen, Z.; Chiaro, B.; Collins, R.; Courtney, W.; Dunsworth, A.; Farhi, E.; Foxen, B.; Fowler, A.; Gidney, C.; Giustina, M.; Graff, R.; Guerin, K.; Habegger, S.; Harrigan, M. P.; Hartmann, M. J.; Ho, A.; Hoffmann, M.; Huang, T.; Humble, T. S.; Isakov, S. V.; Jeffrey, E.; Jiang, Z.; Kafri, D.; Kechedzhi, K.; Kelly, J.; Klimov, P. V.; Knysh, S.; Korotkov, A.; Kostritsa, F.; Landhuis, D.; Lindmark, M.; Lucero, E.; Lyakh, D.; Mandrà, S.; McClean, J. R.; McEwen, M.; Megrant, A.; Mi, X.; Michielsen, K.; Mohseni, M.; Mutus, J.; Naaman, O.; Neeley, M.; Neill, C.; Niu, M. Y.; Ostby, E.; Petukhov, A.; Platt, J. C.; Quintana, C.; Rieffel, E. G.; Roushan, P.; Rubin, N. C.; Sank, D.; Satzinger, K. J.; Smelyanskiy, V.; Sung, K. J.; Trevithick, M. D.; Vainsencher, A.; Villalonga, B.; White, T.; Yao, Z. J.; Yeh, P.; Zalcman, A.; Neven, H.; Martinis, J. M. Quantum supremacy using a programmable superconducting processor. *Nature* **2019**, *574*, 505–510.
- (8) Gong, M.; Wang, S.; Zha, C.; Chen, M.-C.; Huang, H.-L.; Wu, Y.; Zhu, Q.; Zhao, Y.; Li, S.; Guo, S.; Qian, H.; Ye, Y.; Chen, F.; Ying, C.; Yu, J.; Fan, D.; Wu, D.; Su, H.;

- Deng, H.; Rong, H.; Zhang, K.; Cao, S.; Lin, J.; Xu, Y.; Sun, L.; Guo, C.; Li, N.; Liang, F.; Bastidas, V. M.; Nemoto, K.; Munro, W. J.; Huo, Y.-H.; Lu, C.-Y.; Peng, C.-Z.; Zhu, X.; Pan, J.-W. Quantum walks on a programmable two-dimensional 62-qubit superconducting processor. *Science* **2021**, *372*, 948–952.
- (9) Xu, S.; Sun, Z.-Z.; Wang, K.; Xiang, L.; Bao, Z.; Zhu, Z.; Shen, F.; Song, Z.; Zhang, P.; Ren, W.; Zhang, X.; Dong, H.; Deng, J.; Chen, J.; Wu, Y.; Tan, Z.; Gao, Y.; Jin, F.; Zhu, X.; Zhang, C.; Wang, N.; Zou, Y.; Zhong, J.; Zhang, A.; Li, W.; Jiang, W.; Yu, L.-W.; Yao, Y.; Wang, Z.; Li, H.; Guo, Q.; Song, C.; Wang, H.; Deng, D.-L. Digital Simulation of Projective Non-Abelian Anyons with 68 Superconducting Qubits. *Chin. Phys. Lett.* **2023**, *40*, 60301–060301.
- (10) Google Quantum AI, Suppressing quantum errors by scaling a surface code logical qubit. *Nature* **2023**, *614*, 676–681.
- (11) Peruzzo, A.; McClean, J.; Shadbolt, P.; Yung, M.-H.; Zhou, X.-Q.; Love, P. J.; Aspuru-Guzik, A.; O’Brien, J. L. A variational eigenvalue solver on a photonic quantum processor. *Nat. Commun.* **2014**, *5*, 4213.
- (12) O’Malley, P. J. J.; Babbush, R.; Kivlichan, I. D.; Romero, J.; McClean, J. R.; Barends, R.; Kelly, J.; Roushan, P.; Tranter, A.; Ding, N.; Campbell, B.; Chen, Y.; Chen, Z.; Chiaro, B.; Dunsworth, A.; Fowler, A. G.; Jeffrey, E.; Lucero, E.; Megrant, A.; Mutus, J. Y.; Neeley, M.; Neill, C.; Quintana, C.; Sank, D.; Vainsencher, A.; Wenner, J.; White, T. C.; Coveney, P. V.; Love, P. J.; Neven, H.; Aspuru-Guzik, A.; Martinis, J. M. Scalable quantum simulation of molecular energies. *Phys. Rev. X* **2016**, *6*, 031007.
- (13) Cerezo, M.; Arrasmith, A.; Babbush, R.; Benjamin, S. C.; Endo, S.; Fujii, K.; McClean, J. R.; Mitarai, K.; Yuan, X.; Cincio, L.; Coles, P. J. Variational quantum algorithms. *Nat. Rev. Phys.* **2021**, *3*, 625–644.
- (14) Tilly, J.; Chen, H.; Cao, S.; Picozzi, D.; Setia, K.; Li, Y.; Grant, E.; Wossnig, L.;

- Rungger, I.; Booth, G. H.; Tennyson, J. The variational quantum eigensolver: a review of methods and best practices. *Phys. Rep.* **2022**, *986*, 1–128.
- (15) Aspuru-Guzik, A.; Dutoi, A. D.; Love, P. J.; Head-Gordon, M. Simulated quantum computation of molecular energies. *Science* **2005**, *309*, 1704–1707.
- (16) Lee, S.; Lee, J.; Zhai, H.; Tong, Y.; Dalzell, A. M.; Kumar, A.; Helms, P.; Gray, J.; Cui, Z.-H.; Liu, W.; Kastoryano, M.; Babbush, R.; Preskill, J.; Reichman, D. R.; Campbell, E. T.; Valeev, E. F.; Lin, L.; Chan, G. K.-L. Evaluating the evidence for exponential quantum advantage in ground-state quantum chemistry. *Nature Commun.* **2023**, *14*, 1952.
- (17) Bartlett, R. J.; Kucharski, S. A.; Noga, J. Alternative coupled-cluster ansätze II. The unitary coupled-cluster method. *Chem. Phys. Lett.* **1989**, *155*, 133–140.
- (18) Kutzelnigg, W. Error analysis and improvements of coupled-cluster theory. *Theor. Chim. Acta* **1991**, *80*, 349–386.
- (19) Anand, A.; Schleich, P.; Alperin-Lea, S.; Jensen, P. W.; Sim, S.; Díaz-Tinoco, M.; Kottmann, J. S.; Degroote, M.; Izmaylov, A. F.; Aspuru-Guzik, A. A quantum computing view on unitary coupled cluster theory. *Chem. Soc. Rev.* **2022**,
- (20) Lee, J.; Huggins, W. J.; Head-Gordon, M.; Whaley, K. B. Generalized unitary coupled cluster wave functions for quantum computation. *J. Chem. Theory and Comput.* **2018**, *15*, 311–324.
- (21) Grimsley, H. R.; Economou, S. E.; Barnes, E.; Mayhall, N. J. An adaptive variational algorithm for exact molecular simulations on a quantum computer. *Nat. Commun.* **2019**, *10*, 1–9.
- (22) Elfving, V. E.; Millaruelo, M.; Gámez, J. A.; Gogolin, C. Simulating quantum chemistry

- in the seniority-zero space on qubit-based quantum computers. *Phys. Rev. A* **2021**, *103*, 032605.
- (23) Kandala, A.; Mezzacapo, A.; Temme, K.; Takita, M.; Brink, M.; Chow, J. M.; Gambetta, J. M. Hardware-efficient variational quantum eigensolver for small molecules and quantum magnets. *Nature* **2017**, *549*, 242–246.
- (24) Ollitrault, P. J.; Miessen, A.; Tavernelli, I. Molecular quantum dynamics: A quantum computing perspective. *Acc. Chem. Res.* **2021**, *54*, 4229–4238.
- (25) Li, Y.; Benjamin, S. C. Efficient variational quantum simulator incorporating active error minimization. *Phys. Rev. X* **2017**, *7*, 021050.
- (26) Yuan, X.; Endo, S.; Zhao, Q.; Li, Y.; Benjamin, S. C. Theory of variational quantum simulation. *Quantum* **2019**, *3*, 191.
- (27) Colless, J. I.; Ramasesh, V. V.; Dahlen, D.; Blok, M. S.; Kimchi-Schwartz, M. E.; McClean, J. R.; Carter, J.; de Jong, W. A.; Siddiqi, I. Computation of molecular spectra on a quantum processor with an error-resilient algorithm. *Phys. Rev. X* **2018**, *8*, 011021.
- (28) Kandala, A.; Temme, K.; Córcoles, A. D.; Mezzacapo, A.; Chow, J. M.; Gambetta, J. M. Error mitigation extends the computational reach of a noisy quantum processor. *Nature* **2019**, *567*, 491–495.
- (29) Rice, J. E.; Gujarati, T. P.; Motta, M.; Takeshita, T. Y.; Lee, E.; Latone, J. A.; Garcia, J. M. Quantum computation of dominant products in lithium–sulfur batteries. *J. Chem. Phys.* **2021**, *154*, 134115.
- (30) Gao, Q.; Jones, G. O.; Motta, M.; Sugawara, M.; Watanabe, H. C.; Kobayashi, T.; Watanabe, E.; Ohnishi, Y.-y.; Nakamura, H.; Yamamoto, N. Applications of quantum

- computing for investigations of electronic transitions in phenylsulfonyl-carbazole TADF emitters. *npj Comput. Mater.* **2021**, 7, 70.
- (31) Kirsopp, J. J.; Di Paola, C.; Manrique, D. Z.; Krompiec, M.; Greene-Diniz, G.; Guba, W.; Meyder, A.; Wolf, D.; Strahm, M.; Muñoz Ramo, D. Quantum computational quantification of protein-ligand interactions. *Int. J. Quantum Chem.* **2022**, 122, e26975.
- (32) Mitarai, K.; Negoro, M.; Kitagawa, M.; Fujii, K. Quantum circuit learning. *Phys. Rev. A* **2018**, 98, 032309.
- (33) Schuld, M.; Bergholm, V.; Gogolin, C.; Izaac, J.; Killoran, N. Evaluating analytic gradients on quantum hardware. *Phys. Rev. A* **2019**, 99, 032331.
- (34) Zhang, S.-X.; Allcock, J.; Wan, Z.-Q.; Liu, S.; Sun, J.; Yu, H.; Yang, X.-H.; Qiu, J.; Ye, Z.; Chen, Y.-Q.; Lee, C.-K.; Zheng, Y.-C.; Jian, S.-K.; Yao, H.; Hsieh, C.-Y.; Zhang, S. Tensorcircuit: A quantum software framework for the NISQ era. *Quantum* **2023**, 7, 912.
- (35) Chen, J.; Cheng, H.-P.; Freericks, J. K. Quantum-inspired algorithm for the factorized form of unitary coupled cluster theory. *J. Chem. Theory and Comput.* **2021**, 17, 841–847.
- (36) Kottmann, J. S.; Anand, A.; Aspuru-Guzik, A. A feasible approach for automatically differentiable unitary coupled-cluster on quantum computers. *Chem. Sci.* **2021**, 12, 3497–3508.
- (37) Rubin, N. C.; Gunst, K.; White, A.; Freitag, L.; Throssell, K.; Chan, G. K.-L.; Babush, R.; Shiozaki, T. The Fermionic Quantum Emulator. *Quantum* **2021**, 5, 568.
- (38) Lee, C.-K.; Hsieh, C.-Y.; Zhang, S.; Shi, L. Simulation of Condensed-Phase Spec-

- troscopy with Near-Term Digital Quantum Computers. *J. Chem. Theory and Comput.* **2021**, *17*, 7178–7186.
- (39) Lee, C.-K.; Zhong Lau, J. W.; Shi, L.; Kwek, L. C. Simulating energy transfer in molecular systems with digital quantum computers. *J. Chem. Theory and Comput.* **2022**, *18*, 1347–1358.
- (40) Ollitrault, P. J.; Mazzola, G.; Tavernelli, I. Nonadiabatic molecular quantum dynamics with quantum computers. *Phys. Rev. Lett.* **2020**, *125*, 260511.
- (41) Lee, C.-K.; Hsieh, C.-Y.; Zhang, S.; Shi, L. Variational Quantum Simulation of Chemical Dynamics with Quantum Computers. *J. Chem. Theory and Comput.* **2022**, *18*, 2105–2113.
- (42) Jordan, P.; Wigner, E. Über das Paulische Äquivalenzverbot. *Zeitschrift für Physik* **1928**, *47*, 631–651.
- (43) Bravyi, S. B.; Kitaev, A. Y. Fermionic quantum computation. *Ann. Phys.* **2002**, *298*, 210–226.
- (44) Seeley, J. T.; Richard, M. J.; Love, P. J. The Bravyi-Kitaev transformation for quantum computation of electronic structure. *J. Chem. Phys.* **2012**, *137*, 224109.
- (45) Sawaya, N. P.; Menke, T.; Kyaw, T. H.; Johri, S.; Aspuru-Guzik, A.; Guerreschi, G. G. Resource-efficient digital quantum simulation of d -level systems for photonic, vibrational, and spin- s Hamiltonians. *npj Quantum Inf.* **2020**, *6*, 1–13.
- (46) Nam, Y.; Chen, J.-S.; Pienti, N. C.; Wright, K.; Delaney, C.; Maslov, D.; Brown, K. R.; Allen, S.; Amini, J. M.; Apisdorf, J.; Beck, K. M.; Blinov, A.; Chaplin, V.; Chmielewski, M.; Collins, C.; Debnath, S.; Hudek, K. M.; Ducore, A. M.; Keesan, M.; Kreikemeier, S. M.; Mizrahi, J.; Solomon, P.; Williams, M.; Wong-Campos, J. D.;

- Moehring, D.; Monroe, C.; Kim, J. Ground-state energy estimation of the water molecule on a trapped-ion quantum computer. *npj Quantum Inf.* **2020**, *6*, 33.
- (47) Li, W.; Huang, Z.; Cao, C.; Huang, Y.; Shuai, Z.; Sun, X.; Sun, J.; Yuan, X.; Lv, D. Toward practical quantum embedding simulation of realistic chemical systems on near-term quantum computers. *Chem. Sci.* **2022**, *13*, 8953–8962.
- (48) Guo, S.; Sun, J.; Qian, H.; Gong, M.; Zhang, Y.; Chen, F.; Ye, Y.; Wu, Y.; Cao, S.; Liu, K.; Zha, C.; Ying, C.; Zhu, Q.; Huang, H.-L.; Zhao, Y.; Li, S.; Wang, S.; Yu, J.; Fan, D.; Wu, D.; Su, H.; Deng, H.; Rong, H.; Li, Y.; Zhang, K.; Chung, T.-H.; Liang, F.; Lin, J.; Xu, Y.; Sun, L.; Guo, C.; Li, N.; Huo, Y.-H.; Peng, C.-Z.; Lu, C.-Y.; Yuan, X.; Zhu, X.; Pan, J.-W. Experimental quantum computational chemistry with optimised unitary coupled cluster ansatz. *arXiv preprint arXiv:2212.08006* **2022**,
- (49) Wecker, D.; Hastings, M. B.; Troyer, M. Progress towards practical quantum variational algorithms. *Phys. Rev. A* **2015**, *92*, 042303.
- (50) Miessen, A.; Ollitrault, P. J.; Tavernelli, I. Quantum algorithms for quantum dynamics: a performance study on the spin-boson model. *Phys. Rev. Res.* **2021**, *3*, 043212.
- (51) Yao, Y.-X.; Gomes, N.; Zhang, F.; Wang, C.-Z.; Ho, K.-M.; Iadecola, T.; Orth, P. P. Adaptive variational quantum dynamics simulations. *PRX Quantum* **2021**, *2*, 030307.
- (52) Broeckhove, J.; Lathouwers, L.; Kesteloot, E.; Van Leuven, P. On the equivalence of time-dependent variational principles. *Chem. Phys. Lett.* **1988**, *149*, 547–550.
- (53) Qiskit contributors, *Qiskit: An Open-source Framework for Quantum Computing*; IBM, 2023.
- (54) Bergholm, V.; Izaac, J.; Schuld, M.; Gogolin, C.; Ahmed, S.; Ajith, V.; Sohaib Alam, M.; Alonso-Linaje, G.; AkashNarayanan, B.; Asadi, A.; Arrazola, J. M.;

- Azad, U.; Banning, S.; Blank, C.; Bromley, T. R.; Cordier, B. A.; Ceroni, J.; Delgado, A.; Di Matteo, O.; Dusko, A.; Garg, T.; Guala, D.; Hayes, A.; Hill, R.; Ijaz, A.; Isacsson, T.; Ittah, D.; Jahangiri, S.; Jain, P.; Jiang, E.; Khandelwal, A.; Kottmann, K.; Lang, R. A.; Lee, C.; Loke, T.; Lowe, A.; McKiernan, K.; Meyer, J. J.; Montañez-Barrera, J. A.; Moyard, R.; Niu, Z.; O’Riordan, L. J.; Oud, S.; Panigrahi, A.; Park, C.-Y.; Polatajko, D.; Quesada, N.; Roberts, C.; Sá, N.; Schoch, I.; Shi, B.; Shu, S.; Sim, S.; Singh, A.; Strandberg, I.; Soni, J.; Száva, A.; Thabet, S.; Vargas-Hernández, R. A.; Vincent, T.; Vitucci, N.; Weber, M.; Wierichs, D.; Wiersema, R.; Willmann, M.; Wong, V.; Zhang, S.; Killoran, N. PennyLane: Automatic differentiation of hybrid quantum-classical computations. *arXiv preprint arXiv:1811.04968* **2018**,
- (55) MindQuantum Developer, MindQuantum, version 0.6.0. 2021; <https://gitee.com/mindspore/mindquantum> (Accessed May 29, 2023).
- (56) Kottmann, J. S.; Alperin-Lea, S.; Tamayo-Mendoza, T.; Cervera-Lierta, A.; Lavigne, C.; Yen, T.-C.; Verteletskyi, V.; Schleich, P.; Anand, A.; Degroote, M.; Chaney, S.; Kesibi, M.; Curnow, N. G.; Solo, B.; Tsilimigkounakis, G.; Zendejas-Morales, C.; Izmaylov, A. F.; Aspuru-Guzik, A. Tequila: A platform for rapid development of quantum algorithms. *Quantum Sci. Technol.* **2021**, *6*, 024009.
- (57) Fan, Y.; Liu, J.; Zeng, X.; Xu, Z.; Shang, H.; Li, Z.; Yang, J. Q² Chemistry: A quantum computation platform for quantum chemistry. *arXiv preprint arXiv:2208.10978* **2022**,
- (58) Stair, N. H.; Evangelista, F. A. QFort: An efficient state-vector emulator and quantum algorithms library for molecular electronic structure. *J. Chem. Theory and Comput.* **2022**, *18*, 1555–1568.
- (59) Cao, C.; Hu, J.; Zhang, W.; Xu, X.; Chen, D.; Yu, F.; Li, J.; Hu, H.-S.; Lv, D.; Yung, M.-H. Progress toward larger molecular simulation on a quantum computer:

- Simulating a system with up to 28 qubits accelerated by point-group symmetry. *Phys. Rev. A* **2022**, *105*, 062452.
- (60) Schollwöck, U. The density-matrix renormalization group in the age of matrix product states. *Ann. Phys.* **2011**, *326*, 96–192.
- (61) Shang, H.; Fan, Y.; Shen, L.; Guo, C.; Liu, J.; Duan, X.; Li, F.; Li, Z. Towards practical and massively parallel quantum computing emulation for quantum chemistry. *npj Quantum Inf.* **2023**, *9*, 33.
- (62) Ollitrault, P. J.; Baiardi, A.; Reiher, M.; Tavernelli, I. Hardware efficient quantum algorithms for vibrational structure calculations. *Chem. Sci.* **2020**, *11*, 6842–6855.
- (63) Bradbury, J.; Frostig, R.; Hawkins, P.; Johnson, M. J.; Leary, C.; Maclaurin, D.; Necula, G.; Paszke, A.; VanderPlas, J.; Wanderman-Milne, S.; Zhang, Q. JAX: composable transformations of Python+NumPy programs. 2018; <http://github.com/google/jax> (Accessed May 29, 2023).
- (64) Sun, Q.; Berkelbach, T. C.; Blunt, N. S.; Booth, G. H.; Guo, S.; Li, Z.; Liu, J.; McClain, J.; Sayfutyarova, E. R.; Sharma, S.; Wouters, S.; Chan, G. K.-L. PySCF: the Python-based simulations of chemistry framework. *Wiley Interdiscip. Rev. Comput. Mol. Sci.* **2018**, *8*, e1340.
- (65) Luo, X.-Z.; Liu, J.-G.; Zhang, P.; Wang, L. Yao. jl: Extensible, efficient framework for quantum algorithm design. *Quantum* **2020**, *4*, 341.
- (66) Ren, J.; Li, W.; Jiang, T.; Wang, Y.; Shuai, Z. The RENORMALIZER Package. <https://github.com/shuaigroup/Renormalizer>. 2021; <https://github.com/shuaigroup/Renormalizer> (Accessed May 29, 2023).
- (67) McClean, J. R.; Rubin, N. C.; Sung, K. J.; Kivlichan, I. D.; Bonet-Monroig, X.; Cao, Y.; Dai, C.; Fried, E. S.; Gidney, C.; Gimby, B.; Gokhale, P.; Häner, T.; Hardikar, T.;

- Havlíček, V.; Higgott, O.; Huang, C.; Izaac, J.; Jiang, Z.; Liu, X.; McArdle, S.; Neeley, M.; O’Brien, T.; O’Gorman, B.; Ozfidan, I.; Radin, M. D.; Romero, J.; Sawaya, N. P. D.; Senjean, B.; Setia, K.; Sim, S.; Steiger, D. S.; Steudtner, M.; Sun, Q.; Sun, W.; Wang, D.; Zhang, F.; Babbush, R. OpenFermion: The electronic structure package for quantum computers. *Quantum Sci. Technol.* **2020**, *5*, 034014.
- (68) McArdle, S.; Mayorov, A.; Shan, X.; Benjamin, S.; Yuan, X. Digital quantum simulation of molecular vibrations. *Chem. Sci.* **2019**, *10*, 5725–5735.
- (69) Colbert, D. T.; Miller, W. H. A novel discrete variable representation for quantum mechanical reactive scattering via the *S*-matrix Kohn method. *J. Chem. Phys.* **1992**, *96*, 1982–1991.
- (70) Li, W.; Ren, J.; Huai, S.; Cai, T.; Shuai, Z.; Zhang, S. Efficient quantum simulation of electron-phonon systems by variational basis state encoder. *Phys. Rev. Res.* **2023**, *5*, 023046.
- (71) Evangelista, F. A.; Chan, G. K.-L.; Scuseria, G. E. Exact parameterization of fermionic wave functions via unitary coupled cluster theory. *J. Chem. Phys.* **2019**, *151*, 244112.
- (72) McClean, J. R.; Boixo, S.; Smelyanskiy, V. N.; Babbush, R.; Neven, H. Barren plateaus in quantum neural network training landscapes. *Nat. Commun.* **2018**, *9*, 4812.
- (73) Choy, B.; Wales, D. J. Molecular Energy Landscapes of Hardware-Efficient Ansatz in Quantum Computing. *J. Chem. Theory and Comput.* **2023**, *19*, 1197–1206.
- (74) Gao, Q.; Nakamura, H.; Gujarati, T. P.; Jones, G. O.; Rice, J. E.; Wood, S. P.; Pistoia, M.; Garcia, J. M.; Yamamoto, N. Computational investigations of the lithium superoxide dimer rearrangement on noisy quantum devices. *J. Phys. Chem. A* **2021**, *125*, 1827–1836.

- (75) Miháliková, I.; Pivoluska, M.; Plesch, M.; Friák, M.; Nagaj, D.; Šob, M. The Cost of Improving the Precision of the Variational Quantum Eigensolver for Quantum Chemistry. *Nanomaterials* **2022**, *12*, 243.
- (76) Markov, I. L.; Shi, Y. Simulating quantum computation by contracting tensor networks. *SIAM J. Comput.* **2008**, *38*, 963–981.
- (77) Liu, Y. A.; Liu, X. L.; Li, F. N.; Fu, H.; Yang, Y.; Song, J.; Zhao, P.; Wang, Z.; Peng, D.; Chen, H.; Guo, C.; Huang, H.; Wu, W.; Chen, D. Closing the "quantum supremacy" gap: achieving real-time simulation of a random quantum circuit using a new Sunway supercomputer. In *Proceedings of the International Conference for High Performance Computing, Networking, Storage and Analysis*. 2021; pp 1–12.
- (78) Pan, F.; Zhang, P. Simulation of quantum circuits using the big-batch tensor network method. *Phys. Rev. Lett.* **2022**, *128*, 030501.
- (79) Noh, K.; Jiang, L.; Fefferman, B. Efficient classical simulation of noisy random quantum circuits in one dimension. *Quantum* **2020**, *4*, 318.
- (80) Cheng, S.; Cao, C.; Zhang, C.; Liu, Y.; Hou, S.-Y.; Xu, P.; Zeng, B. Simulating noisy quantum circuits with matrix product density operators. *Phys. Rev. Res.* **2021**, *3*, 023005.
- (81) Virtanen, P.; Gommers, R.; Oliphant, T. E.; Haberland, M.; Reddy, T.; Cournapeau, D.; Burovski, E.; Peterson, P.; Weckesser, W.; Bright, J.; van der Walt, S. J.; Brett, M.; Wilson, J.; Millman, K. J.; Mayorov, N.; Nelson, A. R. J.; Jones, E.; Kern, R.; Larson, E.; Carey, C. J.; Polat, İ.; Feng, Y.; Moore, E. W.; VanderPlas, J.; Laxalde, D.; Perktold, J.; Cimrman, R.; Henriksen, I.; Quintero, E. A.; Harris, C. R.; Archibald, A. M.; Ribeiro, A. H.; Pedregosa, F.; van Mulbregt, P.; SciPy 1.0 Contributors, SciPy 1.0: Fundamental Algorithms for Scientific Computing in Python. *Nat. Methods* **2020**, *17*, 261–272.

- (82) Yordanov, Y. S.; Arvidsson-Shukur, D. R.; Barnes, C. H. Efficient quantum circuits for quantum computational chemistry. *Phys. Rev. A* **2020**, *102*, 062612.
- (83) Magoulas, I.; Evangelista, F. A. CNOT-Efficient Circuits for Arbitrary Rank Many-Body Fermionic and Qubit Excitations. *J. Chem. Theory Comput.* **2023**, *19*, 822–836.
- (84) Dunning Jr, T. H. Gaussian basis sets for use in correlated molecular calculations. I. The atoms boron through neon and hydrogen. *J. Chem. Phys.* **1989**, *90*, 1007–1023.
- (85) Li, Z.; Liu, X.; Wang, H.; Ashhab, S.; Cui, J.; Chen, H.; Peng, X.; Du, J. Quantum simulation of resonant transitions for solving the eigenproblem of an effective water Hamiltonian. *Phys. Rev. Lett.* **2019**, *122*, 090504.
- (86) Ryabinkin, I. G.; Lang, R. A.; Genin, S. N.; Izmaylov, A. F. Iterative qubit coupled cluster approach with efficient screening of generators. *J. Chem. Theory and Comput.* **2020**, *16*, 1055–1063.
- (87) Hehre, W. J.; Ditchfield, R.; Pople, J. A. Self-consistent molecular orbital methods. XII. Further extensions of Gaussian-type basis sets for use in molecular orbital studies of organic molecules. *J. Chem. Phys.* **1972**, *56*, 2257–2261.
- (88) Hariharan, P. C.; Pople, J. A. The influence of polarization functions on molecular orbital hydrogenation energies. *Theor. Chim. Acta* **1973**, *28*, 213–222.
- (89) Hoy, A.; Bunker, P. R. A precise solution of the rotation bending Schrödinger equation for a triatomic molecule with application to the water molecule. *J. Mol. Spectrosc.* **1979**, *74*, 1–8.
- (90) Sokolov, I. O.; Barkoutsos, P. K.; Ollitrault, P. J.; Greenberg, D.; Rice, J.; Pistoia, M.; Tavernelli, I. Quantum orbital-optimized unitary coupled cluster methods in the strongly correlated regime: Can quantum algorithms outperform their classical equivalents? *J. Chem. Phys.* **2020**, *152*, 124107.

- (91) Knizia, G.; Chan, G. K.-L. Density matrix embedding: A simple alternative to dynamical mean-field theory. *Phys. Rev. Lett.* **2012**, *109*, 186404.
- (92) Knizia, G.; Chan, G. K.-L. Density matrix embedding: A strong-coupling quantum embedding theory. *J. Chem. Theory Comput.* **2013**, *9*, 1428–1432.
- (93) Motta, M.; Ceperley, D. M.; Chan, G. K.-L.; Gomez, J. A.; Gull, E.; Guo, S.; Jiménez-Hoyos, C. A.; Lan, T. N.; Li, J.; Ma, F.; Millis, A. J.; Prokof'ev, N. V.; Ray, U.; Scuseria, G. E.; Sorella, S.; Stoudenmire, E. M.; Sun, Q.; Tupitsyn, I. S.; White, S. R.; Zgid, D.; Zhang, S. Towards the solution of the many-electron problem in real materials: Equation of state of the hydrogen chain with state-of-the-art many-body methods. *Phys. Rev. X* **2017**, *7*, 031059.
- (94) Mineh, L.; Montanaro, A. Solving the Hubbard model using density matrix embedding theory and the variational quantum eigensolver. *Phys. Rev. B* **2022**, *105*, 125117.
- (95) Nielsen, M. A.; Chuang, I. *Quantum computation and quantum information*; Cambridge University Press, 2010.
- (96) Leggett, A. J.; Chakravarty, S.; Dorsey, A. T.; Fisher, M. P.; Garg, A.; Zwerger, W. Dynamics of the dissipative two-state system. *Rev. Mod. Phys.* **1987**, *59*, 1.
- (97) Shuai, Z.; Li, W.; Ren, J.; Jiang, Y.; Geng, H. Applying Marcus theory to describe the carrier transports in organic semiconductors: Limitations and beyond. *J. Chem. Phys.* **2020**, *153*, 080902.
- (98) Kloss, B.; Reichman, D. R.; Tempelaar, R. Multiset matrix product state calculations reveal mobile Franck-Condon excitations under strong Holstein-type coupling. *Phys. Rev. Lett.* **2019**, *123*, 126601.
- (99) Nan, G.; Yang, X.; Wang, L.; Shuai, Z.; Zhao, Y. Nuclear tunneling effects of charge transport in rubrene, tetracene, and pentacene. *Phys. Rev. B* **2009**, *79*, 115203.

Supplementary Materials for TenCirChem: An Efficient Quantum Computational Chemistry Package for the NISQ Era

Weitang Li,^{*,†} Jonathan Allcock,[‡] Lixue Cheng,[†] Shi-Xin Zhang,[†] Yu-Qin Chen,[†]
Jonathan P. Mailoa,[†] Zhigang Shuai,^{¶,§} and Shengyu Zhang^{*,‡}

[†]*Tencent Quantum Lab, Shenzhen, 518057, China*

[‡]*Tencent Quantum Lab, Hongkong, 999077, China*

[¶]*Department of Chemistry, Tsinghua University, Beijing, 100084, China*

[§]*School of Science and Engineering, The Chinese University of Hong Kong, Shenzhen,
518172, China*

E-mail: liw31@gmail.com; shengyzhang@tencent.com

S1 Review of UCC ansatz

We start with the general expression

$$|\Psi(\theta)\rangle_{\text{UCC}} := \prod_{k=N_{\text{ex}}}^1 e^{\theta_k G_k} |\phi\rangle. \quad (1)$$

S1.1 UCCSD

For the most common case of single and double excitations, the G_k has the form

$$G_k = \begin{cases} a_p^\dagger a_q - \text{h.c.}, \\ a_p^\dagger a_q^\dagger a_r a_s - \text{h.c.} \end{cases} \quad (2)$$

In this case, the disentangled UCC ansatz – which is known as the UCCSD ansatz – has the form

$$|\Psi(\theta)\rangle_{\text{UCCSD}} := \prod_{pqrs} e^{\theta_{pqrs}(a_p^\dagger a_q^\dagger a_r a_s - \text{h.c.})} \prod_{pq} e^{\theta_{pq}(a_p^\dagger a_q - \text{h.c.})} |\phi\rangle . \quad (3)$$

If the number of spin-orbitals is N , then the number of gates in the corresponding circuit scales as $\mathcal{O}(N^4)$.¹

S1.2 k -UpCCGSD

This is a variant of the UCC ansatz which satisfies both high accuracy and low ($\mathcal{O}(N^2)$) gate count requirements.² Here “G”, “p” and “ k ” stand for generalized excitation, paired double excitations, and repeating the ansatz k times, respectively. By pairing double excitations, the number of double excitations is reduced from $\mathcal{O}(N^4)$ to $\mathcal{O}(N^2)$. More specifically, the ansatz has the form

$$|\Psi(\theta)\rangle_{k\text{-UpCCGSD}} := \prod_{l=1}^k \prod_{pq} e^{\theta_{kpq}^{(2)}(a_{p\alpha}^\dagger a_{p\beta}^\dagger a_{q\beta} a_{q\alpha} - \text{h.c.})} \prod_{rs} e^{\theta_{krs}^{(1)}(a_r^\dagger a_s - \text{h.c.})} |\phi\rangle . \quad (4)$$

Here $a_{p\alpha}^\dagger a_{p\beta}^\dagger a_{q\beta} a_{q\alpha}$ means spin-paired double excitations from the q -th spatial orbital to the p -th spatial orbital.

S1.3 pUCCD

This is an efficient ansatz requiring only $\mathcal{O}(N)$ circuit depth and half as many qubits as other UCC ansätze.³⁻⁶ pUCCD allows only paired double excitations, which enables one qubit to represent one spatial orbital instead of one spin orbital, and removes the need to perform the fermion-qubit mapping. Thus, the $\mathcal{O}(N^2)$ excitations can be executed on a quantum computer efficiently using a compact circuit with a linear depth of Givens-SWAP gates.⁴ The Hamiltonian also takes a simpler form in this case, with only N^2 terms:

$$H = \sum_p h_p c_p^\dagger c_p + \sum_{pq} v_{pq} c_p^\dagger c_q + \sum_{p \neq q} w_{pq} c_p^\dagger c_p c_q^\dagger c_q + E_{\text{nuc}} , \quad (5)$$

where $h_p = 2h_{pp}$, $v_{pq} = (pq|pq)$ and $w_{pq} = 2(pp|qq) - (pq|pq)$. Here p and q are indices for spatial orbitals. A drawback of this ansatz is its compromised accuracy, which is comparable to the doubly occupied configuration interaction (DOCI) method⁷ in quantum chemistry.

S2 Conventions

In this section, we introduce the conventions used in TENCIRCHEM, particularly for static electronic structure problems.

Excitations. TENCIRCHEM uses tuples to denote unitary fermionic excitations:

- (p, q) : denotes single excitations $a_p^\dagger a_q - a_q^\dagger a_p$
- (p, q, r, s) : denotes double excitations $a_p^\dagger a_q^\dagger a_r a_s - a_s^\dagger a_r^\dagger a_q a_p$

Higher-order excitations are handled similarly. e.g., a k -th order excitation is represented by a tuple of length $2k$, with the first half corresponding to the excitation operators, and the second half corresponding to the annihilation operators, and Hermitian conjugation is implied, e.g., (p, q, r, s, t, u) denotes $a_p^\dagger a_q^\dagger a_r^\dagger a_s^\dagger a_t a_u - \text{h.c.}$

Spin-orbital indexing. Spin orbitals are indexed from 0 and ordered according to the following rules:

- Beta (down) spins first, followed by alpha (up) spins
- Low energy orbitals first, followed by high energy orbitals

Qubit indexing. Qubits are numbered from 0, with multi-qubit registers numbered with the zeroth qubit on the left, e.g. $|0\rangle_{q_0} |1\rangle_{q_2} |0\rangle_{q_2}$. Unless necessary, we will omit subscripts and use a more compact notation e.g. $|010\rangle$ to denote multi-qubit states. In quantum circuit diagrams qubit numbers increase downwards, starting from qubit zero at the top. Throughout, we assume the Jordan-Wigner encoding where the occupancy of spin-orbital i (using the above ordering) corresponds to the state of qubit $N - 1 - i$ where N is the total number of qubits. In other words, the qubit ordering is reversed spin-orbitals ordering.

The conventions described above are summarized in Fig. S1, taking a 4-electron and 4-orbital system as an example. Following the qubit indexing convention above, the restricted Hartree-Fock (HF) state for such a system is represented as 00110011 in bitstring form. The highest orbital with α -spin comes first in the bitstring, and the lowest orbital with β -spin comes last. In quantum chemistry language, 00110011 refers to a configuration with orbitals 5, 4, 1, and 0 occupied, while in quantum computing language, 00110011 refers to a direct product state with the 2nd, 3rd, 6th, and 7th qubits in state $|1\rangle$ and the rest in state $|0\rangle$. Upon application of the excitation operator (6, 2, 0, 4), the HF state transforms to 01100110.

S3 `print_summary` output

In this section, we provide an overview of the output by the `print_summary` command (see Code Snippet 1). This summary is divided into a number of blocks:

```

1 ##### Ansatz #####
2 #qubits #params #excitations initial condition
3      4      2      3      RHF
4 ##### Circuit #####
5 #qubits #gates #CNOT #multicontrol depth #FLOP

```

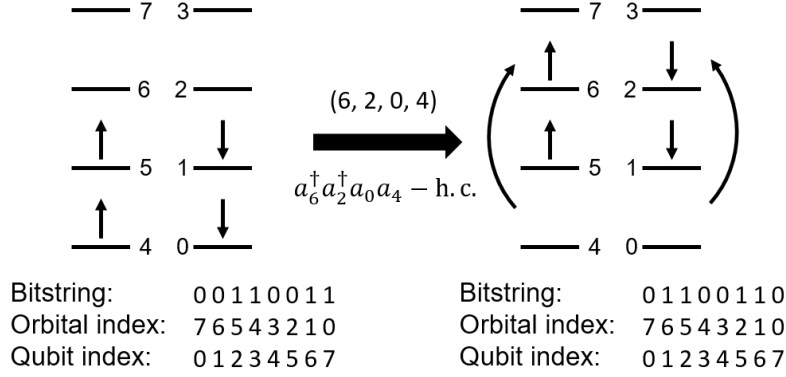


Figure S1: An example of the conventions used for excitations, orbital indexing, and qubit indexing. The HF state of a 4 electron, 4 orbital system is represented as bitstring 00110011. The state is excited to 01100110 via the excitation operator $(6, 2, 0, 4)$.

```

6      4      15      10      1      9 2160
7 ##### Energy #####
8      energy (Hartree)  error (mH)  correlation energy (%)
9 HF      -1.116706      20.568268      -0.000
10 MP2     -1.129868      7.406850      63.989
11 CCSD     -1.137275     -0.000165      100.001
12 UCCSD     -1.137274      0.000000      100.000
13 FCI      -1.137274      0.000000      100.000
14 ##### Excitations #####
15      excitation configuration      parameter  initial guess
16 0      (3, 2)      1001  1.082849e-16      0.000000
17 1      (1, 0)      0110  1.082849e-16      0.000000
18 2  (1, 3, 2, 0)      1010 -1.129866e-01      -0.072608
19 ##### Optimization Result #####
20      e: -1.1372744055294384
21      fun: array(-1.13727441)
22      hess_inv: <2x2 LbfgsInvHessProduct with dtype=float64>
23      init_guess: [0.0, -0.07260814651571333]
24      jac: array([-9.60813938e-19, -1.11022302e-16])
25      message: 'CONVERGENCE: NORM_OF_PROJECTED_GRADIENT_<=_PGTOL'
26      nfev: 6
27      nit: 4
28      njev: 6
29      opt_time: 0.02926015853881836
30      staging_time: 4.5299530029296875e-06
31      status: 0
32      success: True
33      x: array([ 1.08284918e-16, -1.12986561e-01])

```

Code Snippet S1: UCCSD ansatz applied to the H_2 molecule: output of the `print_summary` command.

Ansatz (lines 1-3). From here we see that the UCCSD ansatz is mapped (via the Jordan-Wigner transformation) to a variational quantum circuit on 4 qubits, with two tunable

parameters. The circuit corresponds to 3 excitation operators, which are detailed in the `Excitations` block of the summary. The fact that there are only two tunable parameters for three excitation operators is due to symmetry.

Circuit (lines 4-6). This block details the number of quantum gates that the Jordan-Wigner transformed ansatz is compiled to. By default, `TENCIRCHEM` uses the efficient circuit decomposition of⁸ for circuit compilation. The circuit depth is estimated using `QISKIT` and, as the running time of computing this estimate can be non-negligible for large circuits, the `include_circuit=True` option is by default `False`. The floating point operation count (FLOP) required to calculate the circuit statevector via tensor network contraction is estimated by the `OPT_EINSUM` package⁹ using the default greedy contraction path-finding algorithm.

Note that, in the absence of noise, computing the output of the circuit does not require the circuit to first be decomposed explicitly into gates. Instead, `TENCIRCHEM` makes use of *UCC factor expansion* (See Sec. S5.1) to perform this computation more efficiently. However, if one wishes to simulate noisy quantum circuits – corresponding, for instance, to realistic quantum hardware – then an explicit gate decomposition is necessary.

Energy (lines 7-13). This block includes the final UCCSD energy corresponding to the optimized parameter values, as well as other benchmark energies computed by `PySCF` at Hartree–Fock, second-order Møller–Plesset perturbation theory (MP2), CCSD, and FCI levels of theory.

Excitations (lines 14-18). This block gives further details on the ansatz, which takes the form

$$e^{\theta_2 G_2} e^{\theta_1 G_1} e^{\theta_0 G_0} |\text{HF}\rangle ,$$

where θ_0 is set to be equal to θ_1 due to symmetry, and where

$$\begin{aligned} G_0 &= a_2^\dagger a_3 - a_3^\dagger a_2, \\ G_1 &= a_0^\dagger a_1 - a_1^\dagger a_0, \\ G_2 &= a_0^\dagger a_2^\dagger a_3 a_1 - a_1^\dagger a_3^\dagger a_2 a_0. \end{aligned}$$

The convention for spin-orbital indices is described in Sec. S2. The minimum energy found corresponds to parameter values of $\theta_0 = \theta_1 = 1.05 \times 10^{-16}$ and $\theta_2 = -1.13 \times 10^{-1}$. These final values were obtained from initial guesses of 0, 0, -0.0726 respectively, which correspond to the MP2 excitation amplitudes. The configuration bitstrings obtained after applying each excitation to $|\text{HF}\rangle$ are also given here. Note that the Hermitian conjugation part of the excitation operator annihilates $|\text{HF}\rangle$ and thus has no effect. For comparison, the configuration bitstring corresponding to the Hartree-Fock state is 0101.

Optimization Result (lines 19-33). This block gives details of the procedure used to optimize the ansatz parameters, including the number of iterations required (`nit: 3`) as well as the final energy obtained for the UCCSD ansatz (`e: -1.137...`).

S4 The UCC classes: advanced features

S4.1 User-specified UCC ansätze

UCCSD, k -UpCCGSD, and pUCCD are all special cases of UCC, where the excitations are restricted to take a certain form. No setup is required for these three kinds of ansatz from users: once imported they can be used directly, e.g., via `PUCCD(h2).kernel()`.

More general UCC ansätze can be defined by directly specifying the corresponding excitations. This could be helpful, for instance, in investigating new quantum computational chemistry algorithms. In Sec. S4.4, we will illustrate the power of this approach by imple-

menting the ADAPT-VQE¹⁰ using TENCIRCHEM, and we first provide a simpler example and implement the PUCCD ansatz from scratch (see Code Snippet 2).

```

1 import numpy as np
2 from tencirchem import UCC, PUCCD
3 from tencirchem.molecule import h4
4
5 puccd = PUCCD(h4)
6 ucc = UCC(h4)
7
8 # only paired excitations are included
9 ucc.ex_ops = [
10     (6, 2, 0, 4),
11     (7, 3, 0, 4),
12     (6, 2, 1, 5),
13     (7, 3, 1, 5),
14 ]
15
16 e1 = puccd.kernel()
17 # evaluate UCC energy using the PUCCD circuit parameter
18 e2 = ucc.energy(puccd.params)
19 # e1 is the same as e2
20 np.testing.assert_allclose(e1, e2, atol=1e-6)

```

Code Snippet S2: Implementing the PUCCD ansatz from scratch by using a custom UCC ansatz.

Here, a UCC class with only paired excitations is used to reproduce the PUCCD class for the H₄ molecule. The configuration is done by directly setting the `ex_ops` attribute with tuples for the excitations. `param_ids` and `initial_guess` can be set similarly and the full [Python script](#) is available online. Although internally the UCC class uses a quantum circuit of 8 qubits for simulation and the PUCCD class uses only 4 qubits because of the restriction of paired excitations, the corresponding energies with the same set of circuit parameters are exactly the same. If custom UCC with paired excitation is desired, the UCC class can be initialized with the `hcb=True` argument. For the index of the spin-orbitals and excitation operators, Fig. S1 is a helpful reference.

S4.2 Active Space Approximation

As NISQ quantum hardware is limited in the number of qubits available, the active space approximation is frequently adopted to reduce the problem size.^{5,11–15} In many cases, inner shell molecular orbitals can be treated at the mean-field level without significant loss of accu-

racy, and this approximation is thus also sometimes dubbed the frozen core approximation. Denote the set of frozen occupied spin-orbitals by Ω . The frozen core provides an effective repulsion potential V^{eff} to the remaining electrons

$$V_{pq}^{\text{eff}} = \sum_{m \in \Omega} ([mm|pq] - [mp|qm]). \quad (6)$$

The frozen core also bears the mean-field core energy which effectively modifies the core energy E_{nuc}

$$E_{\text{core}} = E_{\text{nuc}} + \sum_{m \in \Omega} h_{mm} + \frac{1}{2} \sum_{m,n \in \Omega} ([mm|nn] - [mn|nm]). \quad (7)$$

Thus, the *ab initio* Hamiltonian is rewritten as

$$H = \sum_{pq} (h_{pq} + V_{pq}^{\text{eff}}) a_p^\dagger a_q + \sum_{pqrs} h_{pqrs} a_p^\dagger a_q^\dagger a_r a_s + E_{\text{core}}, \quad (8)$$

where p, q, r and s refer to spin-orbitals not included in Ω .

Making use of an active space approximation in TENCIRCHEM is straightforward :

```
1 from tencirchem import UCCSD
2 from tencirchem.molecule import h8
3 # (2e, 2o) active space
4 uccsd = UCCSD(h8, active_space=(2, 2))
5 uccsd.kernel()
6 uccsd.print_summary()
```

Code Snippet S3: UCCSD calculation of H_8 with (2e, 2o) active space approximation. Note that the electron integrals in the active space are readily accessible via `uccsd.int1e` and `uccsd.int2e`.

S4.3 Engines, Backends, and GPU

Different engines can be specified by the `engine` argument, e.g.,

```
1 from tencirchem import UCCSD
2 from tencirchem.molecule import h4
3 uccsd = UCCSD(h4, engine="civector-large")
4 print(uccsd.kernel())
5 print(uccsd.energy(engine="tensornetwork"))
```

and, similar to TENSORCIRCUIT, computational backends can be switched at runtime as

follows:

```
1 from tencirchem import set_dtype, set_backend
2 set_dtype("complex64")
3 set_backend("cupy")
```

There are two ways to use GPUs with TENCIRCHEM. The first is to set the backend to "cupy". The second is to set the backend to "jax" and make sure that CUDA support for JAX is properly configured.

S4.4 Code Example: Implementing ADAPT-VQE

In this section, we illustrate how to use TENCIRCHEM to build novel algorithms by implementing ADAPT-VQE.¹⁰ The complete [Jupyter Notebook](#) tutorial is available online. The first step of the algorithm is to construct an excitation operator pool, as shown below. Here we use all of the single and double excitations as described in Eq. 2. Operators with the same parameter are grouped together in the operator pool so as to prevent spin contamination.

```
1 from tencirchem import UCC
2 from tencirchem.molecule import h4
3
4 ucc = UCC(h4)
5
6 # get all single and double excitations
7 # param_id maps operators to parameters (some operators share the same parameter)
8 ex1_ops, ex1_param_ids, _ = ucc.get_ex1_ops()
9 ex2_ops, ex2_param_ids, _ = ucc.get_ex2_ops()
10
11 # group the operators to form an operator pool
12 from collections import defaultdict
13 op_pool = defaultdict(list)
14 for ex1_op, ex1_id in zip(ex1_ops, ex1_param_ids):
15     op_pool[(1, ex1_id)].append(ex1_op)
16 for ex2_op, ex2_id in zip(ex2_ops, ex2_param_ids):
17     op_pool[(2, ex2_id)].append(ex2_op)
18 op_pool = list(op_pool.values())
```

Code Snippet S4: Construction of an operator pool for the ADAPT-VQE algorithm.

Once the operator pool is formed, ADAPT-VQE constructs the ansatz by selecting operators in the pool iteratively, with new operators chosen to maximize the absolute energy gradient. That is, suppose the ansatz wavefunction at a certain point in the process is $|\psi\rangle$

and the operator selected is G_k , then the new ansatz, defined to be

$$|\Psi\rangle = e^{\theta_k G_k} |\psi\rangle, \quad (9)$$

has a corresponding energy gradient

$$\frac{\partial \langle E \rangle}{\partial \theta_k} = 2 \langle \Psi | H G_k | \Psi \rangle. \quad (10)$$

ADAPT-VQE selects G_k from the operator pool such that

$$\left. \frac{\partial \langle E \rangle}{\partial \theta_k} \right|_{\theta_k=0} = 2 \langle \psi | H G_k | \psi \rangle \quad (11)$$

is maximized. If multiple operators sharing the same parameter are added at the same time, then their gradients are added together. The iterative process by which the ansatz is constructed terminates when the norm of the gradient vector falls below a predefined threshold ϵ .

In the following, $|\psi\rangle$ is obtained by `ucc.civector()` as a vector in the configuration interaction space. `ucc.hamiltonian(psi)` applies H onto $|\psi\rangle$ and `ucc.apply_excitation` applies G_k onto $|\psi\rangle$.

```

1 import numpy as np
2
3 ucc.ex_ops = []
4 ucc.params = []
5 ucc.param_ids = []
6
7 MAX_ITER = 100
8 EPSILON = 1e-3
9 for i in range(MAX_ITER):
10     # calculate gradient of each operator from the pool
11     op_gradient_list = []
12     psi = ucc.civector()
13     bra = ucc.hamiltonian(psi)
14     for op_list in op_pool:
15         grad = bra.conj() @ ucc.apply_excitation(psi, op_list[0])
16         if len(op_list) == 2:
17             grad += bra.conj() @ ucc.apply_excitation(psi, op_list[1])
18         op_gradient_list.append(2 * grad)
19     if np.linalg.norm(op_gradient_list) < EPSILON:
20         break
21     chosen_op_list = op_pool[np.argmax(np.abs(op_gradient_list))]
```

```

22 # update ansatz and run calculation
23 ucc.ex_ops.extend(chosen_op_list)
24 ucc.params = list(ucc.params) + [0]
25 ucc.param_ids.extend([len(ucc.params) - 1] * len(chosen_op_list))
26 ucc.init_guess = ucc.params
27 ucc.kernel()

```

Code Snippet S5: Implementation of the ADAPT-VQE iteration. The complete tutorial is available online as a [Jupyter Notebook](#).

S5 Efficient UCC circuit simulation algorithms

We now introduce the algorithm behind efficient UCC circuit simulation that makes TENCIRCHEM capable of accurately simulating deep UCC circuits with more than 32 qubits. We will first introduce the UCC factor expansion technique, which forms the backbone of the "civector" engine. We then move on to an efficient algorithm to evaluate energy gradients with respect to circuit parameters and other implementation details.

S5.1 UCC factor expansion

In this section, we introduce the UCC factor expansion technique used to achieve efficient simulations of UCC circuits in TENCIRCHEM. Benchmark results are included in the main text. We emphasize that the techniques described in this section are specific for efficiently simulating an ideal circuit *classically*, but are not applicable (without large overhead costs) for real hardware or noisy circuit simulations.

S5.1.1 Traditional approach.

Recall that the general UCC ansatz can be written as $|\Psi\rangle = \prod_{k=N_{\text{ex}}}^1 e^{\theta_k G_k} |\phi\rangle$. To compile each UCC factor $e^{\theta_k G_k}$ into a quantum circuit, the traditional approach is to transform G_k (in the remainder of this section we will refer to G_k simply as G) into commutable Pauli strings, and then simulate each Pauli string via Hamiltonian evolution. Another approach is the YAB method described in the main text, which relies on multi-qubit controlled rotations.

The "tensornetwork" engine follows the YAB method to simulate the UCC circuit.

S5.1.2 Factor expansion approach.

In the more efficient "civector" engine, we use a different approach to classically simulate the UCC circuit, which involves expanding each UCC factor into a polynomial form, implementable only on a classical computer. While this formalism has been published multiple times in a variety of contexts,^{16–18} to the best of our knowledge, TENCIRCHEM is the first package to use such a technique for large-scale UCC circuit simulation.

In the most general case, G can be written as $G = g - g^\dagger$, with

$$g_{j_1 \dots j_m}^{i_1 \dots i_m} = a_{i_1}^\dagger \dots a_{i_m}^\dagger a_{j_1} \dots a_{j_m}, \quad (12)$$

where m is the order of the excitation. $g^\dagger g$ is a projector onto the space that is not annihilated by g .¹⁸

$$(g_{j_1 \dots j_m}^{i_1 \dots i_m})^\dagger g_{j_1 \dots j_m}^{i_1 \dots i_m} = (1 - n_{i_1}) \dots (1 - n_{i_m}) n_{j_1} \dots n_{j_m}, \quad (13)$$

where n is the occupation number operator. It follows that $g^\dagger g g^\dagger = g^\dagger$. Using this equation, together with $g g = g^\dagger g^\dagger = 0$, it is straightforward to show that G has the property

$$G^3 = g^\dagger - g = -G. \quad (14)$$

The corresponding UCC factor can then be expanded as

$$\begin{aligned} e^{\theta G} &= 1 + \theta G + \frac{\theta^2 G^2}{2} - \frac{\theta^3 G}{3!} - \frac{\theta^4 G^2}{4!} + \frac{\theta^5 G}{5!} + \dots \\ &= 1 + G^2 + \sum_{j=0} \frac{(-1)^j \theta^{2j+1}}{(2j+1)!} G - \sum_{j=0} \frac{(-1)^j \theta^{2j}}{(2j)!} G^2 \\ &= 1 + \sin \theta G + (1 - \cos \theta) G^2 \end{aligned} \quad (15)$$

In the special case of $G^2 = -I$, the famous formula $e^{\theta G} = \cos \theta + \sin \theta G$ is recovered.

Supposing $|\psi\rangle$ is any intermediate state during circuit execution, multiplying $|\psi\rangle$ with Eq. 15 yields

$$e^{\theta G} |\psi\rangle = |\psi\rangle + \sin \theta G |\psi\rangle + (1 - \cos \theta) G^2 |\psi\rangle. \quad (16)$$

Thus, to evaluate $e^{\theta G} |\psi\rangle$ it is sufficient to evaluate $G |\psi\rangle$ and $G^2 |\psi\rangle$.

The advantages of using Eq. 16 compared to the traditional approaches are twofold. First, Eq. 15 significantly saves on the number of matrix multiplications required to simulate $e^{\theta G} |\psi\rangle$. Second, as both G and G^2 conserve particle numbers in the up and down spin sectors, TENCIRCHEM is able to store $|\psi\rangle$ in the particle-number conserving space instead of the whole Fock space, just as in the standard FCI calculation. Thus, in the following, we use configuration interaction space to denote this particle-number conserving sector of the Fock space. In traditional UCC circuit simulations, where each quantum gate is realized by matrix multiplication, storing wavefunction in configuration interaction space is not possible because a single H gate or X gate is able to destroy the particle number conserving property.

Representing the quantum state in configuration interaction space greatly reduces the memory requirements for UCC simulation. A closed-shell molecule with N spatial orbitals and M electrons has Fock space of dimension 2^{2N} . In contrast, the number of possible configurations in each spin sector is $C_{M/2}^N$, and the dimension of its configuration interaction space is only $\left(C_{M/2}^N\right)^2$. In addition, because G and $|\phi\rangle$ are both real, $|\psi\rangle$ can be represented by real numbers rather than complex numbers in classical computers. In Table S1, we list the memory requirements to represent wavefunctions in configuration interaction spaces and Fock spaces for several values of N and M . While the required memory using configuration interaction space still scales exponentially, in practice the memory saving compared with using Fock space is significant, particularly so when $|N - M|$ is large.

Table S1: Memory requirements to represent system wavefunctions in configuration interaction space and Fock space. In configuration interaction space each amplitude is stored by a 64-bit floating-point number and in Fock space each amplitude is stored by a 128-bit complex number.

N	M	Configuration Interaction Space		Fock Space		Memory Saving
		Dimension	Memory	Dimension	Memory	
2	2	4	32 B	16	256 B	8x
4	2	16	128 B	256	4.1 kB	32x
	4	36	288 B			14x
8	4	784	6.3 kB	65,536	1.0 MB	167x
	8	4,900	39.2 kB			27x
16	8	3,312,400	26.5 MB	4,294,967,296	68.7 GB	2,593x
	16	165,636,900	1.3 GB			52x
48	4	1,272,384	10.1 MB	7.9×10^{28}	1.3 QB	1.2×10^{23} x

S5.2 Gradients with respect to circuit parameters

TENCIRCHEM uses an efficient algorithm to calculate the energy gradient with respect to the parameters.¹⁹ The algorithm is applicable to the "civector" engine, and for the "tensornetwork" engine traditional auto-differentiation is implemented. For $j = 1, 2, \dots, N_{ex}$ define

$$|\psi_j\rangle = \prod_{k=j}^1 e^{\theta_k G_k} |\phi\rangle, \quad (17)$$

and $|\psi'_j\rangle$

$$\langle\psi'_j| = \langle\psi|\hat{H} \prod_{k=N_{ex}}^j e^{\theta_k G_k}, \quad (18)$$

where H is the system Hamiltonian. The energy expectation value can be written as

$$\langle E \rangle = \langle\psi'_{j+1}|\psi_j\rangle, \quad (19)$$

and the energy gradient as

$$\frac{\partial\langle E \rangle}{\partial\theta_j} = 2\langle\psi'_{j+1}|G_j|\psi_j\rangle. \quad (20)$$

Once $|\psi\rangle$ is obtained, $\langle\psi_{N_{ex}+1}^{(1)}| = \langle\psi|\hat{H}$ and $|\psi_{N_{ex}}\rangle = |\psi\rangle$ are calculated. The remaining

$\langle\psi'_j|$ and $|\psi_{j-1}\rangle$ are then obtained by the recurrence relation

$$\begin{aligned}\langle\psi'_j| &= \langle\psi'_{j+1}|e^{\theta_j G_j}, \\ |\psi_{j-1}\rangle &= e^{-\theta_j G_j}|\psi_j\rangle,\end{aligned}\tag{21}$$

and, for each $\langle\psi'_j|$ and $|\psi_{j-1}\rangle$ pair, $\frac{\partial\langle E\rangle}{\partial\theta_j}$ is evaluated by Eq. 20. This algorithm thus computes all gradients in one iteration over j , requiring only a constant amount of memory.

S5.3 Other techniques for efficient simulation

With UCC factor expansion and efficient gradient computation, TENCIRCHEM is able to simulate much larger molecular systems compared to traditional simulation packages. TENCIRCHEM also use several other techniques to accelerate calculations. In particular (i) initial values of θ_k are set to the corresponding t_2 amplitudes obtained by MP2, to enable faster convergence; (ii) double excitation operators with t_2 very close to zero are screened out by default because the excitation is likely prohibited by molecular point-group symmetry;²⁰ (iii) double excitation operators are also sorted by t_2 amplitudes to avoid ambiguous ansätze.²¹

References

- (1) O’Gorman, B.; Huggins, W. J.; Rieffel, E. G.; Whaley, K. B. Generalized swap networks for near-term quantum computing. *arXiv preprint arXiv:1905.05118* **2019**,
- (2) Lee, J.; Huggins, W. J.; Head-Gordon, M.; Whaley, K. B. Generalized unitary coupled cluster wave functions for quantum computation. *J. Chem. Theory and Comput.* **2018**, *15*, 311–324.
- (3) Henderson, T. M.; Bulik, I. W.; Scuseria, G. E. Pair extended coupled cluster doubles. *J. Chem. Phys.* **2015**, *142*, 214116.

- (4) Elfving, V. E.; Millaruelo, M.; Gámez, J. A.; Gogolin, C. Simulating quantum chemistry in the seniority-zero space on qubit-based quantum computers. *Phys. Rev. A* **2021**, *103*, 032605.
- (5) O'Brien, T. E.; Anselmetti, G.; Gkritis, F.; Elfving, V. E.; Polla, S.; Huggins, W. J.; Oumarou, O.; Kechedzhi, K.; Abanin, D.; Acharya, R.; Aleiner, I.; Allen, R.; Andersen, T. I.; Anderson, K.; Ansmann, M.; Arute, F.; Arya, K.; Asfaw, A.; Atalaya, J.; Bacon, D.; Bardin, J. C.; Bengtsson, A.; Boixo, S.; Bortoli, G.; Bourassa, A.; Bovaird, J.; Brill, L.; Broughton, M.; Buckley, B.; Buell, D. A.; Burger, T.; Burkett, B.; Bushnell, N.; Campero, J.; Chen, Y.; Chen, Z.; Chiaro, B.; Chik, D.; Cogan, J.; Collins, R.; Conner, P.; Courtney, W.; Crook, A. L.; Curtin, B.; Debroy, D. M.; Demura, S.; Drozdov, I.; Dunsworth, A.; Erickson, C.; Faoro, L.; Farhi, E.; Fatemi, R.; Ferreira, V. S.; Flores Burgos, L.; Forati, E.; Fowler, A. G.; Foxen, B.; Giang, W.; Gidney, C.; Gilboa, D.; Giustina, M.; Gosula, R.; Grajales Dau, A.; Gross, J. A.; Habegger, S.; Hamilton, M. C.; Hansen, M.; Harrigan, M. P.; Harrington, S. D.; Heu, P.; Hilton, J.; Hoffmann, M. R.; Hong, S.; Huang, T.; Huff, A.; Ioffe, L. B.; Isakov, S. V.; Iveland, J.; Jeffrey, E.; Jiang, Z.; Jones, C.; Juhas, P.; Kafri, D.; Kelly, J.; Khattnar, T.; Khezri, M.; Kieferová, M.; Kim, S.; Klimov, P. V.; Klotz, A. R.; Kothari, R.; Korotkov, A. N.; Kostitsa, F.; Kreikebaum, J. M.; Landhuis, D.; Laptev, P.; Lau, K.; Laws, L.; Lee, J.; Lee, K.; Lester, B. J.; Lill, A. T.; Liu, W.; Livingston, W. P.; Lochar, A.; Lucero, E.; Malone, F. D.; Mandra, S.; Martin, O.; Martin, S.; McClean, J. R.; McCourt, T.; McEwen, M.; Megrant, A.; Mi, X.; Mieszala, A.; Miao, K. C.; Mohseni, M.; Montazeri, S.; Morvan, A.; Movassagh, R.; Mruczkiewicz, W.; Naaman, O.; Neeley, M.; Neill, C.; Nersisyan, A.; Neven, H.; Newman, M.; Ng, J. H.; Nguyen, A.; Nguyen, M.; Niu, M. Y.; Omonije, S.; Opremcak, A.; Petukhov, A.; Potter, R.; Pryadko, L. P.; Quintana, C.; Rocque, C.; Roushan, P.; Saei, N.; Sank, D.; Sankaragomathi, K.; Satzinger, K. J.; Schurkus, H. F.; Schuster, C.; Shearn, M. J.; Shorter, A.; Shutt, N.; Shvarts, V.; Skrzynny, J.; Smelyanskiy, V.; Smith, W. C.; Somma, R.; Sterling, G.

- Strain, D.; Szalay, M.; Thor, D.; Torres, A.; Vidal, G.; Villalonga, B.; Vollgraff Heidweiller, C.; White, T.; Woo, B. W. K.; Xing, C.; Yao, Z. J.; Yeh, P.; Yoo, J.; Young, G.; Zalcman, A.; Zhang, Y.; Zhu, N.; Zobrist, N.; Gogolin, C.; Babbush, R.; Rubin, N. C. Purification-based quantum error mitigation of pair-correlated electron simulations. *arXiv preprint arXiv:2210.10799* **2022**,
- (6) Zhao, L.; Goings, J.; Wright, K.; Nguyen, J.; Kim, J.; Johri, S.; Shin, K.; Kyoung, W.; Fuks, J. I.; Rhee, J.-K. K.; Rhee, Y. M. Orbital-optimized pair-correlated electron simulations on trapped-ion quantum computers. *arXiv preprint arXiv:2212.02482* **2022**,
- (7) Weinhold, F.; Wilson Jr, E. B. Reduced density matrices of atoms and molecules. I. The 2 matrix of double-occupancy, configuration-interaction wavefunctions for singlet states. *J. Chem. Phys.* **1967**, *46*, 2752–2758.
- (8) Yordanov, Y. S.; Arvidsson-Shukur, D. R.; Barnes, C. H. Efficient quantum circuits for quantum computational chemistry. *Phys. Rev. A* **2020**, *102*, 062612.
- (9) Daniel, G.; Gray, J. opt_einsum-A Python package for optimizing contraction order for einsum-like expressions. *J. Open Source Softw.* **2018**, *3*, 753.
- (10) Grimsley, H. R.; Economou, S. E.; Barnes, E.; Mayhall, N. J. An adaptive variational algorithm for exact molecular simulations on a quantum computer. *Nat. Commun.* **2019**, *10*, 1–9.
- (11) Reiher, M.; Wiebe, N.; Svore, K. M.; Wecker, D.; Troyer, M. Elucidating reaction mechanisms on quantum computers. *Proc. Natl. Acad. Sci. U.S.A.* **2017**, *114*, 7555–7560.
- (12) Takeshita, T.; Rubin, N. C.; Jiang, Z.; Lee, E.; Babbush, R.; McClean, J. R. Increasing the representation accuracy of quantum simulations of chemistry without extra quantum resources. *Phys. Rev. X* **2020**, *10*, 011004.

- (13) Mizukami, W.; Mitarai, K.; Nakagawa, Y. O.; Yamamoto, T.; Yan, T.; Ohnishi, Y.-y. Orbital optimized unitary coupled cluster theory for quantum computer. *Phys. Rev. Res.* **2020**, *2*, 033421.
- (14) McCaskey, A. J.; Parks, Z. P.; Jakowski, J.; Moore, S. V.; Morris, T. D.; Humble, T. S.; Pooser, R. C. Quantum chemistry as a benchmark for near-term quantum computers. *npj Quantum Inf.* **2019**, *5*, 99.
- (15) Huang, K.; Cai, X.; Li, H.; Ge, Z.-Y.; Hou, R.; Li, H.; Liu, T.; Shi, Y.; Chen, C.; Zheng, D.; Xu, K.; Liu, Z.-B.; Li, Z.; Fan, H.; Fang, W.-H. Variational quantum computation of molecular linear response properties on a superconducting quantum processor. *J. Phys. Chem. Lett.* **2022**, *13*, 9114–9121.
- (16) Chen, J.; Cheng, H.-P.; Freericks, J. K. Quantum-inspired algorithm for the factorized form of unitary coupled cluster theory. *J. Chem. Theory and Comput.* **2021**, *17*, 841–847.
- (17) Kottmann, J. S.; Anand, A.; Aspuru-Guzik, A. A feasible approach for automatically differentiable unitary coupled-cluster on quantum computers. *Chem. Sci.* **2021**, *12*, 3497–3508.
- (18) Rubin, N. C.; Gunst, K.; White, A.; Freitag, L.; Throssell, K.; Chan, G. K.-L.; Babush, R.; Shiozaki, T. The Fermionic quantum emulator. *Quantum* **2021**, *5*, 568.
- (19) Luo, X.-Z.; Liu, J.-G.; Zhang, P.; Wang, L. Yao. jl: Extensible, efficient framework for quantum algorithm design. *Quantum* **2020**, *4*, 341.
- (20) Cao, C.; Hu, J.; Zhang, W.; Xu, X.; Chen, D.; Yu, F.; Li, J.; Hu, H.-S.; Lv, D.; Yung, M.-H. Progress toward larger molecular simulation on a quantum computer: Simulating a system with up to 28 qubits accelerated by point-group symmetry. *Phys. Rev. A* **2022**, *105*, 062452.

- (21) Grimsley, H. R.; Claudino, D.; Economou, S. E.; Barnes, E.; Mayhall, N. J. Is the Trotterized UCCSD ansatz chemically well-defined? *J. Chem. Theory and Comput.* **2019**, *16*, 1–6.